C1. Structural engineering in earthquake zones

THEME C1

Structural Engineering in Earthquake Zones

Structures de génie civil en zones sismiques

Konstruktiver Ingenieurbau in Erdbebengebieten

Chairman: G.F. Fox, USA

Coordinator: M. Virlogeux, France

General Reporter: T.P. Tassios, Greece

The theme has been introduced by the General Reporter in the Introductory Report of the 12th Congress, available at the IABSE Secretariat.

Leere Seite
Blank page
Page vide

Behaviour of Concrete Bridge Piers under Seismic Attack

Comportement de piles de pont sous l'effet de charges sismiques

Verhalten von Stahlbeton-Brückenpfeilern unter Erdbebeneinwirkungen

M.J.N. PRIESTLEY
Reader in Civil Eng.
Univ. of Canterbury
Christchurch, New Zealand

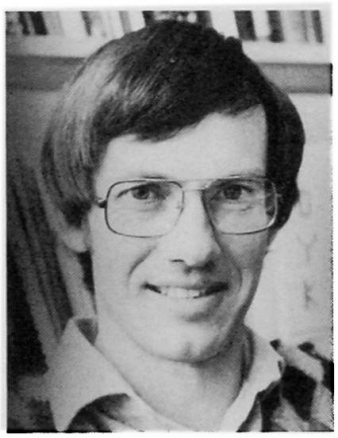

Nigel Priestley, born in 1943, obtained his Ph.D. in Civil Eng. from the Univ. of Canterbury in 1966. After 8 years as Head of the Ministry of Works and Development Structural Testing Laboratory he returned to the Univ. of Canterbury in 1975, specialising in Structural Design. He has published extensively in the fields of seismic design and thermal response of structures.

SUMMARY
The paper summarises recent research in New Zealand into the seismic behaviour of bridge piers. Results are reported for a wide variety of section shapes tested under axial load and bending moment at high displacement ductilities. Design recommendations for bridge piers under seismic loading are presented.

RESUME
Cet article donne un résumé des recherches récentes en Nouvelle Zélande sur le comportement sismique des piles de ponts, et présente les résultats d'expériences sur des piles de formes diverses, soumises à des charges axiales et latérales, avec des grands déplacements ductiles. Des recommandations pour le calcul parasismique des piles sont présentées.

ZUSAMMENFASSUNG
Der Artikel fasst die jüngsten in Neuseeland durchgeführten Untersuchungen des Verhaltens von Brückenpfeilern unter Erdbebeneinwirkung zusammen. Es werden die Ergebnisse von Versuchen an einer Reihe Brückenpfeiler mit verschiedenen Querschnittsformen wiedergegeben, die auf Biegung und Normalkraft bis zum Erreichen grosser plastischer Verformungen belastet wurden. Es werden ferner Empfehlungen für die Bemessung von Brückenpfeilern unter Erdbebenbelastung gemacht.

1. INTRODUCTION

The seismic performance of bridges is a matter of special importance. For effective post-earthquake rescue operations to be mounted, access to the affected area by road or rail is essential. This access can be completely cut by the failure of one or two critical bridges, particularly when rough terrain does not facilitate cross-country mobility. On economic grounds, bridges also assume special importance. The costs of having a rail bridge out of action may exceed US$20,000/hr to the railroad operator. Similar costs, though generally less direct, can be assigned to the loss of a major road bridge, where alternative routes are not available, or involve lengthy detours.

Despite these observations, performance of bridges in severe earthquakes has not been good, with extensive damage being sustained by bridge piers, in particular, and it is only comparatively recently that detailed research has been undertaken to improve seismic design of bridging. This paper summarises an extensive research programme into the seismic performance of bridge piers carried out at the University of Canterbury, New Zealand, over the past 10 years.

2. SEISMIC LOADING: STRENGTH VS DUCTILITY

It is generally uneconomic to design structures to withstand lateral forces corresponding to full elastic response to design-level earthquakes. The alternative, and widely accepted approach is to design for a lower force level, and detail the structure for ductility to ensure it can sustain the inelastic displacements at the design level of seismic attack without significant strength degradation. Frequently, however, codes are not explicit about the interaction between strength and ductility, and the ductility capacity imparted by the specified detailing requirements (if any exist) are not stated.

An approach recently proposed in New Zealand [1] involves specification of inelastic response spectra for clearly identified levels of structural ductility, such as those shown in Fig. 1. The 5% damping spectra apply for a design earthquake of 150 year average return period for the most seismically active regions of New Zealand, and correspond to an expected peak ground acceleration of 0.5g. For periods greater than $T = 0.7s$, inelastic spectra are obtained from the elastic spectrum by dividing the latter by the ductility factor μ, that is, the 'equal-displacement' principle is applied. However, for shorter period structures, the equal-displacement principle is non-conservative, and inelastic spectra C_μ are found from the elastic spectrum C_1 using the expression

$$C_\mu = \frac{0.7\, C_1}{(\mu-1)T + 0.7} \qquad (1)$$

which provides a gradual transition from the equal-displacement approach at $T = 0.7s$, through the equal-energy principle at about $T = 0.3s$, to the equal-acceleration requirement at $T = 0$. The result is inelastic spectra for short period structures that substantially exceed those resulting from codes requiring force-reduction coefficients which are independent of period.

Use of detailed spectra such as those of Fig. 1 implies an ability to assess the ductility capacity of a bridge structure with some accuracy. Design requirements will normally dictate that any inelastic action occurs in the bridge piers, since it is both impractical and undesirable to design for plastic hinges in superstructures, and plastic hinges in piles should be avoided because of difficulties in assessing and repairing damage after an earthquake. Fig. 2 illustrates an idealisation of ductility by representing as equivalent elasto-plastic behaviour. For the majority of bridges, where ductility is provided by flexural plastic hinging of the piers, the ductility cap-

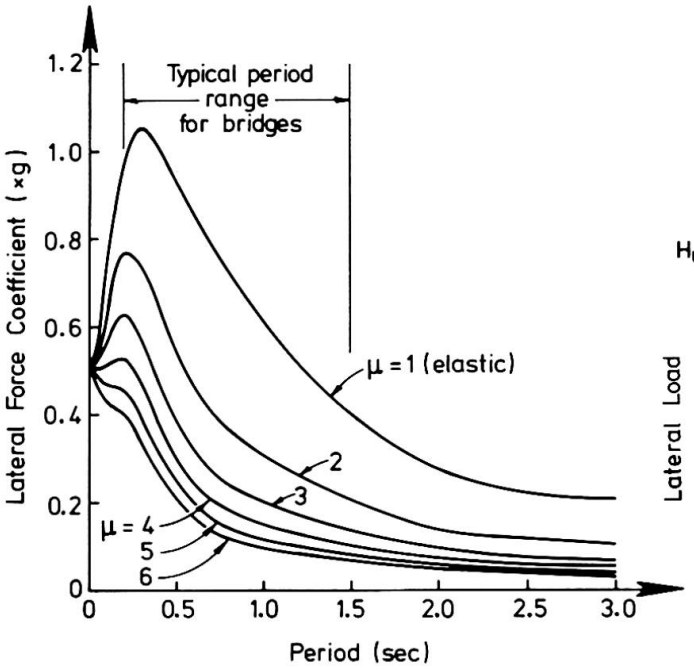

Fig.1 INELASTIC DESIGN SPECTRA FOR 0.5g GROUND ACCELERATION

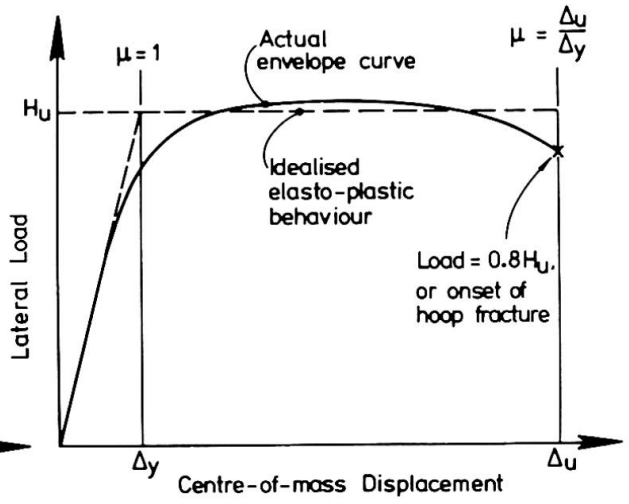

Fig. 2 DEFINITION OF DUCTILITY CAPACITY

acity will be limited by the ultimate displacement Δ_μ of the bridge pier. Definition of Δ_μ is somewhat subjective, but New Zealand practice is to take the displacement corresponding to either first fracture of confining steel (which results in rapid degradation of performance), or to a 20% drop of lateral load capacity as the limit. In assessing the overall structure ductility capacity from the pier inelastic displacement capability, consideration of elastic deformations occurring in foundations and bridge bearings must be made, as these reduce the structure ductility [2].

3. EXPERIMENTAL RESEARCH INTO BRIDGE PIER BEHAVIOUR

In order to obtain the ductilities implied by Fig. 1, compression strains at the extreme compression fibre as high as 2 to 4% may be necessary. As this vastly exceeds the unconfined compression strain of concrete, commonly taken as 0.3-0.4%, confinement in the form of transverse hoops or spirals is required. Research in New Zealand into the strength and ductility of bridge piers has over recent years been directed towards an assessment of the effectiveness of different amounts and configurations of confining reinforcement. The research has involved two phases of testing: axial load testing to investigate the compression stress-strain characteristics of confined concrete, and flexural testing to investigate ductility capacity of sections designed on the basis of stress-strain curves developed in the first phase.

Fig. 3 shows some of the sections that have been tested in the two phases. Section sizes have generally been as large as possible within the load and physical size limitations of a 10 MN capacity DARTEC servohydraulically controlled testing machine used to apply axial load, to facilitate realistic modelling of both concrete and reinforcement.

3.1 Stress-Strain Characteristics of Confined Concrete

For sections tested under axial load only (Fig. 3a) variables have included section shape, longitudinal reinforcement content, lateral reinforcement (confining steel) content and configuration, and loading rate. The relationship between amount and distribution of confining reinforcement and the confined

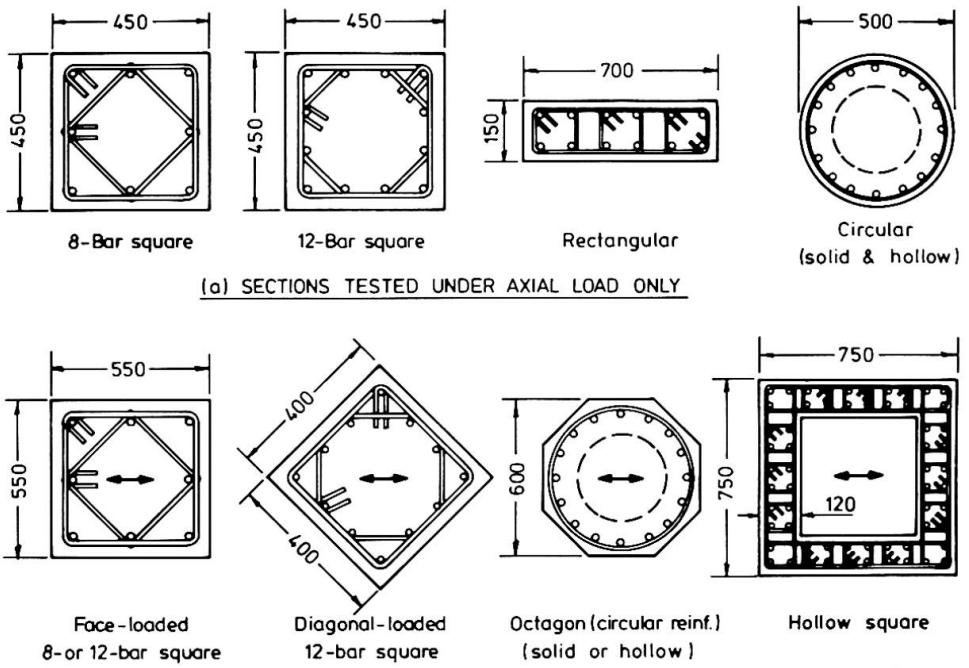

Fig. 3 SECTIONS TESTED TO ESTABLISH DUCTILITY OF BRIDGE PIERS

stress-strain curve has been of particular interest, as has been the influence of loading rate. The design of the DARTEC machine is such that strains can be applied at seismic rates, with the maximum load capacity of 10 MN being attainable in less than 0.3s.

Typical results are shown in Fig. 4 for circular and rectangular sections containing different amounts of confining reinforcement, expressed in terms of volumetric ratio, ρ_s , related to the volume of the confined core [3]. Comparison of confined stress-strain curves with unconfined curves ($\rho_s = 0$) indicates significant increases in compression strength with amount of confinement, and more importantly, very substantial increases in concrete ductility, apparent in the reduced slope of the falling-branch section of the stress-strain curves, and the high strain at which hoop fracture first occurred. Fig. 4a indicates that ultimate compression strains exceeding 5% are attainable, with first hoop fracture indicated by a sudden drop in load capacity near the end of the stress-strain curve.

Mander showed [3] that the experimental curves could be adequately predicted by an analysis based on a '5-parameter' multiaxial failure criteria developed by William and Warkne [4]. This approach resulted in a prediction for maximum confined concrete strength f'_{cc} to be related to the unconfined strength f'_{co} by the expression

$$\frac{f'_{cc}}{f'_{co}} = -1.254 + 2.254\sqrt{1 + 7.94\frac{f'_{\ell}}{f'_{co}}} - 2.0\frac{f'_{\ell}}{f'_{co}} \qquad (2)$$

where f'_{ℓ} is the effective lateral pressure exerted on the core concrete by the confining steel at yield stress. Mander also showed that longitudinal strain at first fracture of confining reinforcement could be predicted by energy considerations, relating the increase in strain energy in compression of the confined concrete to that provided by tensile straining the confining steel to fracture. Theoretical stress-strain curves based on this approach are included for comparison with experimental curves in Fig. 4. It will be observed that very good agreement results.

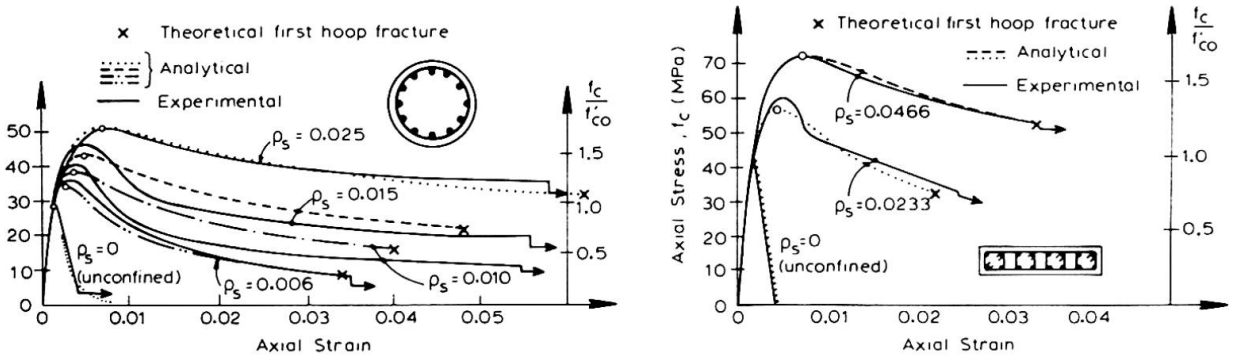

Fig.4 AXIAL STRESS-STRAIN CURVES FOR CONFINED CONCRETE

3.2 Flexural Ductility Under Cyclic Loading

Sections subjected to combined axial load and lateral bending are shown in Fig. 3b. In addition to these sections, smaller octagonal and rectangular sections have been tested to investigate the influence of aspect ratio [column height divided by section thickness or diameter]. Testing involved cyclic reversals of lateral displacement to successive limits of μ = 0.75 , 2, 4, 6 and 8, with two full cycles at each level of ductility [5-8].

Fig. 5 shows typical results for a rectangular column and an octangonal column confined in accordance with provisions presented in section 4 of this paper. It will be noted that the load-displacement hysteresis loops are very stable, with insignificant strength or stiffness degradation between cycles of displacement to the same ductility limit. The results support the use of the μ = 6 inelastic spectrum of Fig. 1 for fully confined columns. Results for square columns loaded parallel to a diagonal, and for hollow rectangular columns have also been satisfactory, but it has been found that thin-walled hollow circular columns with only one ring of longitudinal reinforcement have suffered rapid strength degradation at comparatively low ductilities, particularly when axial load levels were high. Columns with longitudinal reinforcement lapped at the critical (maximum moment) section tended to have reduced ductility capacity because of concentration of plasticity over a very small hinge length adjacent to the critical section.

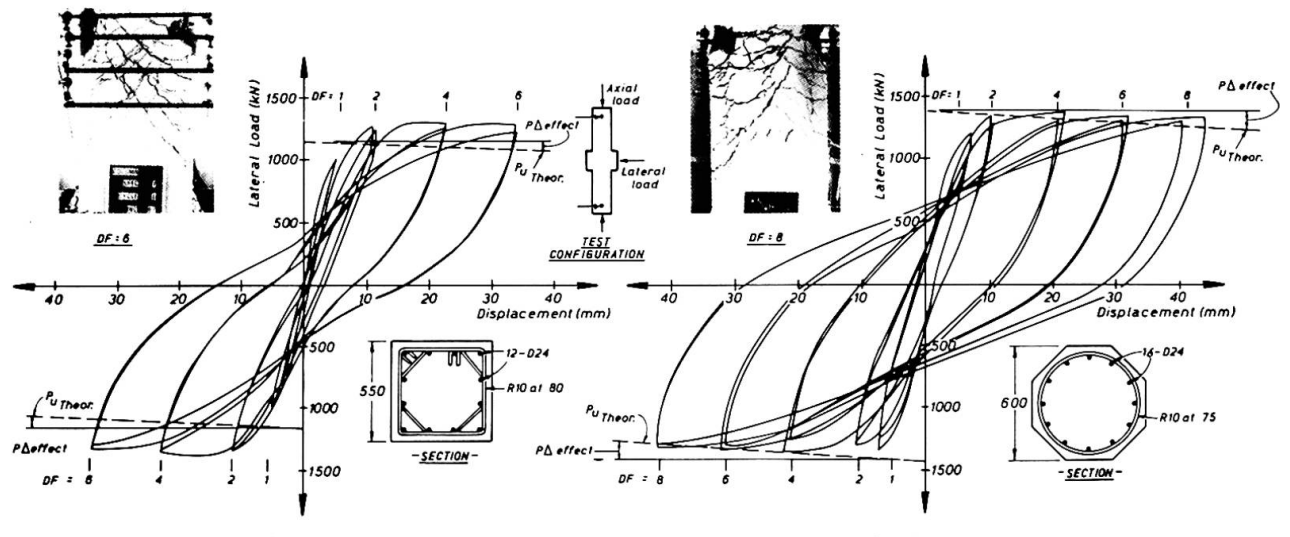

(a) RECTANGULAR COLUMN, $P = 0.26 f'_c A_g$, f'_c = 23MPa, f_y = 300MPa

(b) OCTAGONAL COLUMN, $P = 0.23 f'_c A_g$, f'_c = 30MPa, f_y = 300MPa

FIG. 5 - LOAD-DISPLACEMENT LOOPS FOR FULLY CONFINED COLUMNS

3.3 Shear Strength Under Cyclic Loading

All columns tested under combined axial load and cyclic reversals of bending have attained flexural strengths exceeding 'ideal' capacity based on measured strengths, normal flexural strength equations for concrete, and an ultimate compression strain of 0.3%. This is primarily a result of enhanced concrete compression strength, and strain at maximum moment, resulting from confinement (see Fig. 4). Fig. 6 shows the extent of strength enhancement for a large number of columns as a function of axial load level. Despite considerable scatter, the trend is obvious, with strength enhancement between 50% and 100% for high axial load ratios.

This has significance for shear design. Since the enhanced flexural strength will be developed at the design level earthquake, albeit at a somewhat reduced ductility, the column must be able to support the correspondingly enhanced shear force without developing a brittle shear failure, which exhibits very limited ductility. Current research [9] is investigating the suitability of different approaches, including the ACI method, and a modified form of compression field theory, to predict behaviour of bridge columns failing in shear. Results to date have indicated that the ACI approach is conservative for elastic response, or for very low ductility, but does not give sufficient protection at high ductility levels, when concrete shear resisting mechanisms break down under the cyclic reversals of loading. Typical results are presented in Fig. 7, which compares degradation of shear strength V expressed as a fraction of shear corresponding to flexural hinging, V_{if} , for circular columns identical except for the amount of shear reinforcement, expressed in terms of the volumetric ratio ρ_s . It will be seen that column 12, with $\rho_s = 0.0102$ contained sufficient shear reinforcement to develop the flexural strength (i.e. $V/V_{if} > 1$) but eventually suffered a shear failure at $\mu = 4$. Column 18, with half as much shear reinforcement also initially developed the flexural strength, but suffered shear failure, and rapid strength degradation at $\mu = 1.5$. Column 19, with a lesser amount of shear reinforcement was unable to develop the flexural strength before suffering shear failure. The results indicate that for a given amount of shear reinforcement, the shear strength is a function of the required flexural ductility level.

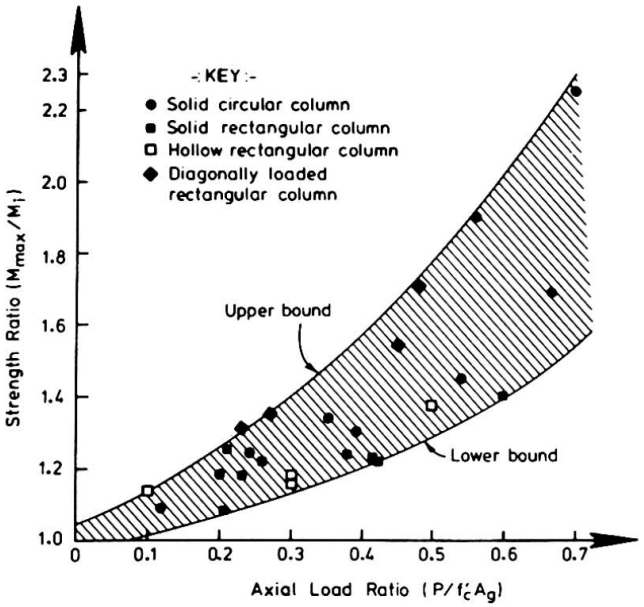

Fig. 6 FLEXURAL STRENGTH ENHANCEMENT OF CONFINED COLUMNS

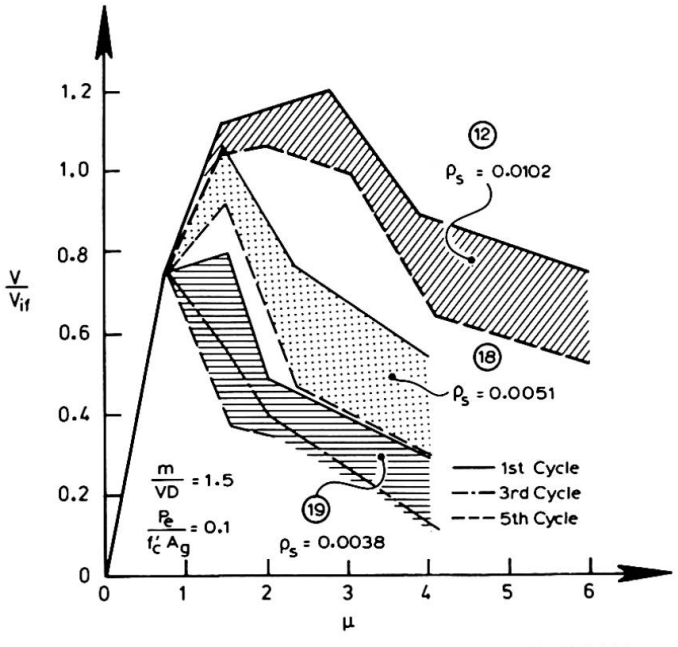

Fig. 7 DEGRADATION OF SHEAR STRENGTH WITH DUCTILITY

4. DESIGN RECOMMENDATIONS

On the basis of the experimental research summarised in the previous section,

New Zealand practice allows design for a ductility of $\mu = 6$, provided the following requirements are met.

1. For column with axial load less than $P = 0.3\ f'_c A_g$, confining reinforcement must be provided for the portion of column subject to more than 80% of the maximum moment, or for a length equal to the section depth, whichever is larger. For axial loads greater than $P = 0.3\ f'_c A_g$, the extent of confinement is increased by 50%.

2. Anchorage of confining steel must be by welding stirrups closed, or bending back into the confined core. Lapping in the cover concrete is not permitted.

3. The maximum spacing of the confining reinforcement along the member axis must not exceed 6 times the longitudinal bar diameter, nor 1/5 of the section width, nor 200 mm. The first requirement is the most important, as longitudinal bar buckling invariably develops at moderate ductility levels when confinement is more widely spaced.

4. The amount of confinement required for full confinement is given by the greater of the two following requirements:

$$A_b = F(0.3s(\frac{A_g}{A_c} - 1)\ \frac{f'_c}{f_{yh}}\ (0.5 + 1.25\ \frac{P_e}{f'_c\ A_g}\ )) \qquad (3)$$

or

$$A_b = F(0.12s\ \frac{f'_c}{f_{yh}}\ (0.5 + 1.25\ \frac{P_e}{f'_c\ A_g}\ )) \qquad (4)$$

where A_g and A_c are the gross and core section areas respectively, s is the axial spacing of hoop sets, or spiral pitch, and f_{yh} is the yield strength of the confining reinforcement. For circular hoops or spirals of bar area A_b, F = one quarter the diameter of the confined core. For rectangular hoops with total bar area A_b [i.e. the sum of areas of all parallel confining legs] in the direction being confined, $F = h$, the width of the confined core.

Expressions (3) and (4) will provide member ductilities of at least $\mu = 8$. For lower ductility demands, the amount of confinement required, As_μ, is

$$As_\mu = As_8\ \frac{(\mu - 2)}{6} \qquad (5)$$

where As_8 is the amount of confinement given by the more stringent of eqns. 3 or 4.

5. Shear strength must exceed the maximum feasible flexural strength, to avoid shear failure.

5. CONCLUSIONS

Extensive testing of large scale models of reinforced concrete bridge piers has established that ductilities of the order of $\mu = 6$ to $\mu = 8$ can be dependably obtained from well confined columns. The design requirements listed in this paper are felt to be the minimum necessary to obtain satisfactory performance at a design ductility level of $\mu = 6$.

6. ACKNOWLEDGEMENTS

Financial support by the Road Research Unit of the N.Z. National Roads Board, and by the University of Canterbury is gratefully acknowledged.

7. REFERENCES

1. BERRILL, J.B., PRIESTLEY, M.J.N., and CHAPMAN, H.E., Design Earthquake Loading and Ductility Demand. Bull. N.Z. National Society for Earthquake Engineering, Vol. 13, No.3, Sept. 1980, pp.232-241.

2. PRIESTLEY, M.J.N. PARK, R., and NG, K.H., Influence of Foundation Compliance on the Seismic Response of Bridge Piers. Bull. NZNSEE, Vol.12, No.1, March 1979, pp.22-34.

3. MANDER, J.B., PRIESTLEY, M.J.N., and PARK, R., Seismic Design of Bridge Piers. Dept. of Civil Eng. Research Report 84-2, University of Canterbury, Feb. 1984, 442 pp & App.

4. WILLIAM, K.J. and WARNKE, E.P., Constitutive Model for the Triaxial Behaviour of Concrete. Proc. IABSE, Vol.19, 1975.

5. PRIESTLEY, M.J.N., PARK, R. and POTANGAROA, R.T., Ductility of Spirally Confined Concrete Columns. Journal, ASCE Struct. Div. Jan. 1981, pp.181-202.

6. PARK, R., PRIESTLEY, M.J.N., and GILL, W.D., Ductility of Square Confined Reinforced Concrete Columns. Journal,ASCE Struct. Div. Vol.108, No.ST4, April 1983, pp.929-950.

7. ANG, B.G., PRIESTLEY, M.J.N., and PARK, R., Ductility of Reinforced Concrete Bridge Piers Under Seismic Loading. Dept. of Civil Eng., Research Report 81-3 , University of Canterbury, Feb. 1981, 109 pp.

8. ZAHN, F.A., PARK. R., and PRIESTLEY, M.J.N., Strength and Ductility of Reinforced Concrete Piers. A Summary Report. Research Report 83-7, University of Canterbury, Dec. 1983, 43 pp.

9. ANG, B.G., Dynamic Shear Strength of Bridge Piers. Ph.D. thesis, University of Canterbury (under preparation).

Advanced Design of Multi-story Reinforced Concrete Building

Conception moderne d'un bâtiment à plusieurs étages en béton armé

Fortschrittlicher Entwurf vielstöckiger Stahlbetongebäude

Toshikazu TAKEDA
Deputy Director
Ohbayashi-Gumi, Ltd.
Tokyo, Japan

Kenzoh YOSHIOKA
Superv. Researcher
Ohbayashi-Gumi, Ltd.
Tokyo, Japan

Hiroaki ETO
Researcher
Ohbayashi-Gumi, Ltd.
Tokyo, Japan

SUMMARY

The design concept and design technique to make a multi-story reinforced concrete building a structure of high earthquake resistance are described, and a 30-story reinforced concrete model building is designed using the technique. The results of dynamic experiments on the frame and static experiments on columns of the model building are given, and it is indicated that the model building possesses ample ductility and excellent earthquake resistance.

RESUME

L'article présente la conception et les techniques de construction employées en vue de rendre hautement résistant aux tremblements de terre un bâtiment élevé en béton armé. Un modèle d'un bâtiment en béton armé de 30 étages est réalisé selon cette technique de construction. Les résultats des essais dynamiques sur le cadre et des essais statiques sur les colonnes de ce modèle sont présentés. La ductilité et la résistance aux tremblements de terre du modèle sont aussi présentées.

ZUSAMMENFASSUNG

Das Entwurfskonzept und die Entwurfstechnik, die zum Bau von vielstöckigen Stahlbetongebäuden mit hoher Widerstandsfähigkeit gegen Erdbeben nötig sind, werden beschrieben, und ein 30-stöckiges Stahlbetongebäude wird unter Verwendung dieser Technik entworfen. Die Ergebnisse der dynamischen Versuche mit dem Rahmen und der statischen Versuche mit den Stützen des modellierten Gebäudes werden beschrieben, und es wird aufgezeigt, dass das Modellgebäude ein grosses Mass an Duktilität besitzt und hervorragende Widerstandsfähigkeit gegen Erdbeben bietet.

1. INTRODUCTION

Multi-story reinforced concrete buildings have been built up to the present in various parts of the world subjected to comparatively severe earthquakes, but it cannot necessarily be said that earthquake-resistant design giving thorough consideration to properties peculiar to reinforced concrete structures has been carried out. In Japan, which is one of the most earthquake-prone countries in the world, it has generally been considered that reinforced concrete construction is inferior in earthquake resistance compared with steel construction and steel and reinforced concrete composite construction, and there have been few cases of construction of multi-story reinforced concrete buildings. However, reinforced concrete construction is a structural form which is amply capable of withstanding large earthquake forces if carefully designed. This paper, taking into consideration the characteristics of reinforced concrete structures, proposes a design concept and a design technique for rendering a multi-story reinforced concrete building into a ductile structure of highly reliable earthquake resistance. A 30-story reinforced concrete model building designed employing this technique is described, and the results of dynamic experiments on the component frames and static experiments of members are presented.

2. STRUCTURAL PLAN AND DESIGN FLOW

2.1 Structural Plan

2.1.1 Total Collapse Form of Beam-Yielding Type

Designing is done to make the building one of pure frame construction for an ultimate collapse form of beam-yielding type having large deformability as shown in Fig. 1. This collapse form is one in which damage from earthquake is not concentrated at a single portion, and instead, the entire building takes on a collapse form, which does not change for the frames of both directions against input of external seismic forces from two directions, and therefore, there is a high margin of safety against earthquake. With a multi-story building, tensile stresses are produced in the outermost columns and ultimate bending strengths are lowered, but designing is done so that a beam-yielding type will result as much as possible even in such case.

2.1.2 Cross-sectional Shape of Beam

As shown in Fig. 2, beams of small depth and large width are adopted to make it easier for plastic flanges to be produced at beam ends along with maintaining adequate shear strengths of beams.

2.1.3 Cross-sectional Shape of Column

Round columns are adopted and spiral hoops are used as shear reinforcement. Actually, in consideration of constructability, the concrete of a column is made octagonal as shown in Fig. 1. A round column using a spiral hoop provides high restraint against the core concrete and main reinforcement of the column, maintains sufficiently large ductility under high axial stresses.

2.1.4 Beam-to-Column Panel

Horizontal haunches are provided at beam-to-column panels as shown in Fig. 3 to secure anchored lengths of main reinforcing bars of beams. The horizontal haunches alleviate slipping phenomena of main reinforcement of beams and are useful for increasing shear strengths of panels.

2.1.5 Considerations of Two-direction Input

(1) Limitations to Axial Stresses of Columns

Corner columns are sometimes subjected to seismic forces in two directions to

result in large axial forces, and therefore, the following limitations are provided:

- Under long-term load: ${}_L\sigma_a \leq 0.2F_c$
- Ultimate: ${}_U\sigma_a = {}_L\sigma_a + 1.5{}_M\sigma_a \leq 0.6F_c$

For columns in general:

- Under long-term load: ${}_L\sigma_a < 0.333F_c$
- Ultimate: ${}_U\sigma_a = {}_L\sigma_a + {}_M\sigma_a < 0.55F_c$

(2) Calculation of Main Reinforcement of Column

The flexure reinforcement at column end is computed using the ultimate strength equation for bending moment 1.5 times that for collapse mechanism in order that the column will not yield even when subjected to input from two directions and the beam-yielding type collapse form will be maintained as much as possible.

2.1.6 Extra Calculation of Design Shear Forces of Beams and Columns

Design shear stresses are increased by extra amounts as follows in order that adequate ductility, that is, excellent deformability of beams and columns of ultimate ductility factors not less than 6 will be secured.

- Beam: ${}_DQ_G = {}_LQ_G + 1.5{}_MQ_G$
- Column: ${}_DQ_C = 1.5{}_MQ_C$

2.2 Design Flow

The earthquake-resistant design flow of a multi-story reinforced concrete building consisting of a pure frame structure is shown in Fig. 4. Firstly, in preliminary calculations, the cross section is assumed taking into consideration axial stress coefficient σ_0/F_c of the column, and correspondence with the response spectrum, configurations of displacement modes, etc., are verified performing eigenvalue calculations. Next, earthquake loads, namely, base shear coefficient and shear force distribution, are assumed, and in addition, the entire structure is replaced by a one-mass-point system and a prediction is made of the response. If the results are satisfactory, the earthquake load is decided, and the process moves on to primary design. Here, allowable stress intensity designing is done for stresses under long-term load and under earthquake load. Next, a check is made of the axial stresses of columns at beam-yielding type collapse. The strength possessed is calculated carrying out computations of the column cross section by ultimate strength equation.

When the static design above has been completed, a response prediction is again made by the substitute one-mass-point system, and checks are made of displacements. Upon confirming that the results of the checks are satisfactory, the next step is elasto-plastic seismic response analyses, and response analyses by a mass-point system and frame response analyses are performed. It is ascertained by frame response analyses that the ductility factor of the story is not more than 1 for a medium-scale earthquake of 250 gal and not more than 2 for a large earthquake of 400 gal.

3. OUTLINE AND DYNAMIC DESIGN OF MODEL BUILDING

3.1 Outline of Building

The model building made the object of design was a 30-story reinforced concrete residential building, and a pure frame structure of uniform spans of 5.55 m as shown in Figs. 5 and 6. The standard story height was 2.85 m with only the first story 4 m. The columns were octagonal columns using spiral hoops with diameters 95 to 80 cm. Beam depths were the two kinds of 70 cm and 75 cm, with

beam width made a wide 50 cm. Horizontal haunches were provided at beam-to-column panels. The concretes used were normal-weight concrete of F_C = 4,119 - 3,236 N/cm^2 and lightweight concrete of F_C = 2,942 - 2,648 N/cm^2.

3.2 Earthquake Load

Designing was done in accordance with the design flow of Fig. 4. The natural periods of the building determined were as shown in Table 1. The primary natural period was 1.81 sec. Base shear coefficients C_B were 0.08 for exterior columns and corner columns, and 0.1 for interior columns. The design shear forces for the individual stories were determined smoothing out Taft EW of the largest story shear force distribution from elastic earthquake responses of 100 gal as shown in Fig. 7.

3.3 Ultimate Strength Design of Beams and Columns

The cross sections of beams and columns were computed using the ultimate strength equation and the reinforcement quantities were determined. The results are given in Table 2 and Table 3.

3.4 Lumped Mass System Response Analysis

The displacements between stories obtained from lumped mass system responses are shown in Fig. 8. The solid lines in the figure are yielding displacements δ_y. With responses of 250 gal and 400 gal, there are portions of responses exceeding δ_y, or 2 δ_y, but this is allowed considering that smooth response displacements would be obtained if frame analyses are performed.

3.5 Frame Response Analysis

Elasto-plastic earthquake response frame analyses were performed, and the vibration properties of the model building over the elastic and plastic ranges, namely, elasto-plastic behaviors of the entire building, stories, and beams and columns, were studied. Analysis was performed only on Frame Ⓒ, and Hachinohe NS, with highest response level and primary vibration predominant, was used as the input seismic wave. The maximum input acceleration was 400 gal considering a great earthquake.

The distribution of the maximum response values of displacements between stories is shown in Fig. 9. The displacements between stories in frame analyses were largest at the 6th story with 3.06 cm (R = 1/93) and the 21st story with 3.22 cm (R = 1/89). The ductility factors of the stories determined by dividing displacements between stories by yielding displacement of a lumped mass system were μ = 0.52 - 1.88 to be within the range of design target values for ductility factors of stories of not more than 2.

The locations of yielding hinge occurrence of beams and columns in frame analyses and the ductility factors of yielded members are shown in Fig. 10. Except at the bases of the first-story exterior columns where axial forces due to earthquake force are on the tension side, yielding hinges did not occur at columns, with yielding hinges produced at beams in the 1st to 26th stories. The ductility factor μ of a member which had yielded was 1.0 - 3.0, and the target value of $\mu < 4$ was satisfied.

4. STATIC AND DYNAMIC TESTS OF MEMBERS

With the model building as the object, static experiments of columns including panels of beams and columns, and dynamic experiemnts of frames were conducted, and the results are shown below.

4.1 Experiments on Columns Including Beam-and-Column Panels

The specimen is shown in Fig. 11. This specimen considered an interior column at the first story and was approximately one half the size of actual. The column was octagonal, circumscribing a circle of 45-cm diameter, with horizontal haunches provided at the beam-to-column panel. Loading was done as shown in Fig. 12 in order that plastic hinges would be produced at beam ends and column bases to result in a collapse form. Axial forces equal to the limit to axial stress intensity of 0.55 F_C of interior columns described in Chapter 2 were made to act on the columns. The concrete strength of this specimen was F_C = 4,217 N/cm^2. The failure condition and load-deformation curve of the specimen are shown in Figs. 13 and 14. As expected, plastic hinges were produced at column bases and beam ends, and failure occurred in collapse form. There was hardly any strength reduction up to joint translation angle of approximately 1/20, and a large deformability was indicated.

4.2 Dynamic Experiments of 6-Story Frame

Dynamic experiments of a 6-story frame were conducted in order to ascertain the safety during earthquake of a 30-story model building. The specimen is shown in Fig. 15. It is approximately 1/7 of actual in scale, the columns being octagonal to circumscribe circles of 13.5 cm. Beams were of width of 70 mm and depth of 105 mm, with horizontal haunches provided at beam-to-column panels. Added weight of 9 tons was applied to the columns, and axial force of σ_0 = 622 N/cm^2 was made to act. The specimen was a frame taken out from the bending inflection point of the beam, and in order to maintain this portion horizontal during vibration, steel supports were erected at beam ends and the beam and pin joints were provided with the beam. Hachinohe NS seismic waves were made to act on the specimen. From the correspondence between period of specimen, period of 30-story building and seismic waves, the time axis of input seismic wave was reduced to 1/4, and maximum acceleration was considered as 350 gal from the limitations due to the characteristics of the shaking table. The maximum response value is shown in Table 4, and the load-deformation curve, and the measured and calculated values of displacements and acceleration responses in Figs. 16 and 17, respectively. At acceleration of 350 gal, the joint translation angle of the specimen was 1/69, and the ductility factor 1.36.

5. CONCLUSIONS

The building designed according to the design concept indicated here, was recognized to be of amply high earthquake resistance during a strong earthquake according to an example of design of a 30-story reinforced concrete building and the results of experiments on component members of the building.

NOTATIONS

$_L\sigma_0$: axial stress intensity under long-term load
$_M\sigma_0$: axial stress intensity at collapse mechanism
$_U\sigma_0$: ultimate axial stress intensity
F_C: specified concrete strength
$_DQ_G$, $_DQ_C$: design shear forces of beam and column, respectively
$_LQ_G$: shear force under long-term load
$_MQ_G$, $_MQ_C$: shear forces at collapse mechanism of beam and column, respectively

REFERENCE

1) Takeda, T., Yoshioka, K., Eto, H., and Tada, T., "Study on Aseismic Design of High Rise Reinforced Concrete Buildings, (Part 1), (Part 2), (Part 3)," (in Japanese), Trans. of AIJ, Extra, September 1983, pp. 1663-1668.

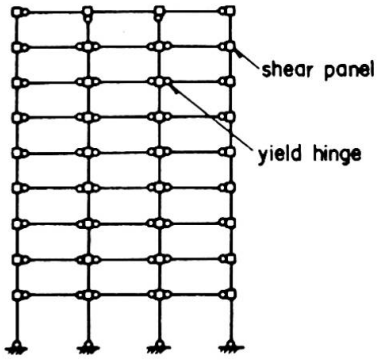

Fig. 1
Frame of Beam-Yielding Type

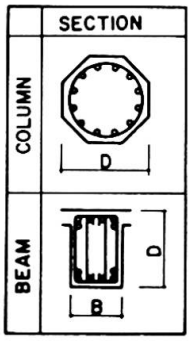

Fig. 2
Cross Section of Column and Beam

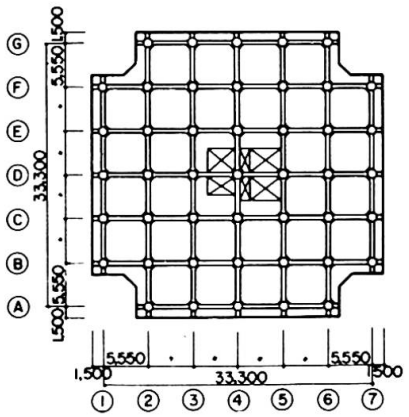

Fig. 5
Prototype Building Plan

Table 1
Natural Period of Prototype Building

T_1 (sec)	T_2 (sec)	T_3 (sec)
1.813	0.838	0.378

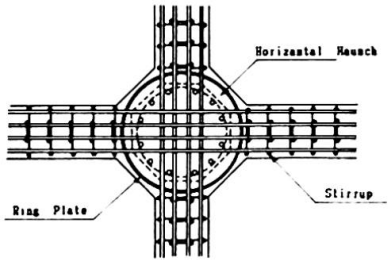

Fig. 3 Column-Beam Connection

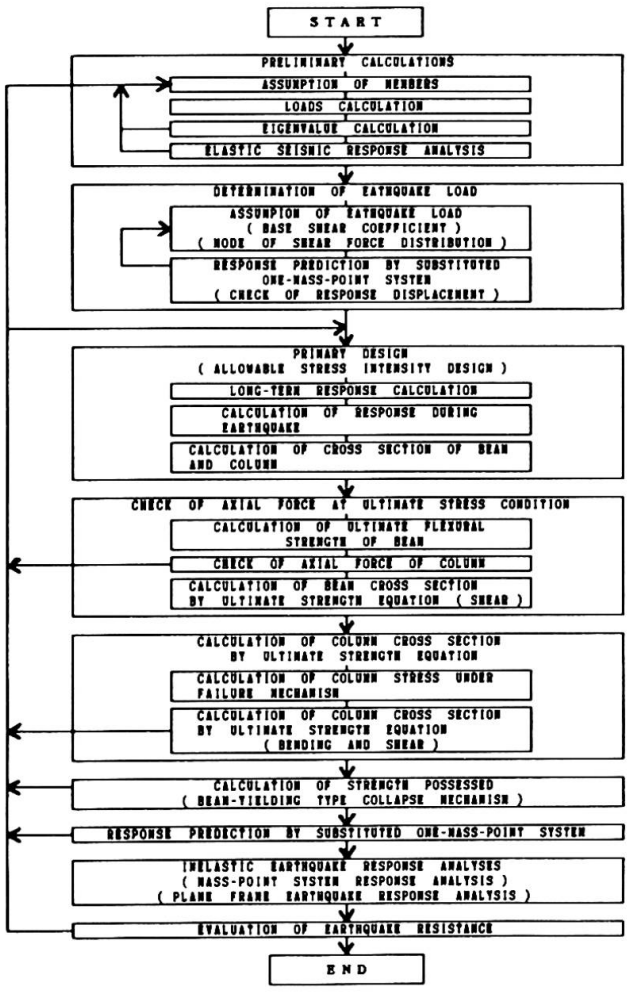

Fig. 4 Design Flow

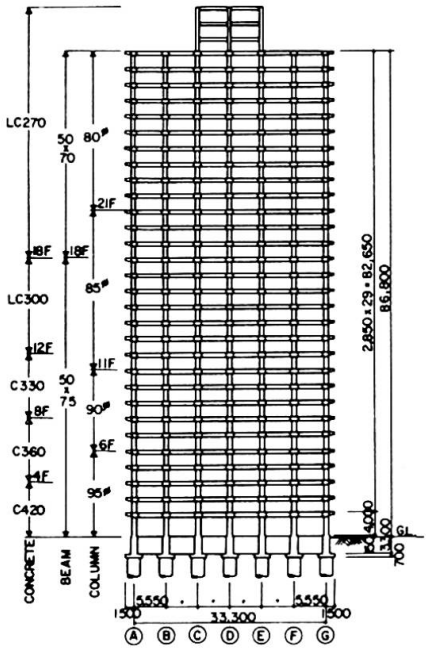

Fig. 6 Prototype Building Section

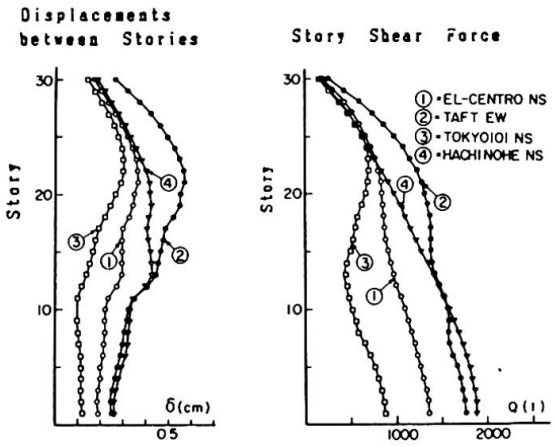

Fig. 7
Displacements between Stories and Story Shear Force Calculated by Elastic Earthquake Response Analysis

Table 2 List of Beams

story	cross section b×D (cm × cm)	location	exterior frame: main reinforcement: exterior end	exterior frame: main reinforcement: interior end	exterior frame: stirrup: tie	interior frame: main reinforcement: both ends	interior frame: stirrup: tie
30 \ 29	50×70	upper	3 - D22	3 - D22	4 - D10 @ 150	5 - D22	4 - D13 @ 150
		lower	2 - D22	2 - D22		4 - D22	
27 \ 25		upper	3 - D25	2 - D25 1 - D22		4 - D25 2 - D22	
		lower	3 - D22	3 - D22		3 - D25 2 - D22	
24 \ 21		upper	2 - D29 2 - D25	3 - D29	4 - D13 @ 150	4 - D29 2 - D25	4 - D10 @ 150
		lower	2 - D25 2 - D22	2 - D25 1 - D22		3 - D29 2 - D25	
20 \ 18		upper	2 - D29 2 - D25	2 - D29 2 - D22		6 - D29	
		lower	2 - D29 1 - D25	2 - D29 1 - D22		5 - D29	
17 \ 11	50×75	upper	2 - D32 2 - D25	2 - D32 1 - D29		2 - D32 4 - D29	
		lower	2 - D29 2 - D22	2 - D29 1 - D22		4 - D29 2 - D25	
10 \ 6		upper	2 - D32 2 - D29	2 - D32 2 - D25		2 - D32 4 - D29	
		lower	2 - D29 2 - D25	3 - D29		4 - D29 2 - D25	
5 \ 1		upper	2 - D32 3 - D25	2 - D32 2 - D29		2 - D32 4 - D29	
		lower	2 - D29 3 - D25	4 - D29		4 - D29 2 - D25	

● main reinforcing bar: SD40, stirrup + tie: SD35
at the both ends of beams ties are provided at the spaces of 100 mm within the zones extent as beam depth

Table 3 List of Columns

story	cross section D (mm)	C_1 (exterior column): main reinforcement	C_1 (exterior column): hoop	C_2 (interior column): main reinforcement	C_2 (interior column): hoop
30 \ 28	80●	12 - D35	spiral hoop D10 @100	12 - D35	spiral hoop D10 @100
27 \ 25					
24 \ 21			spiral hoop D10 @100		spiral hoop D10 @100
20 \ 18	85●				
17 \ 11					spiral hoop D10 @100
10 \ 6	90●		spiral hoop D10 @100		
5 \ 1	95●				

● main reinforcement : SD40, spiral hoop : SD35
At the bottom of columns of the first floor, sub hoops D10 are provided at the spaces of 80mm within the extent of one and half times column diameter

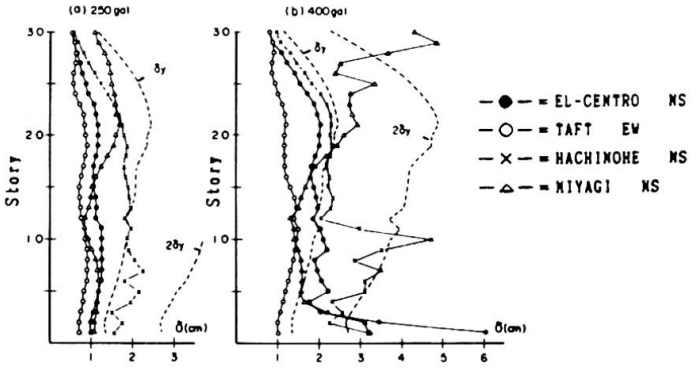

Fig. 8 Displacements between Stories Calculated by Inelastic Mass-Point System Response Analysis

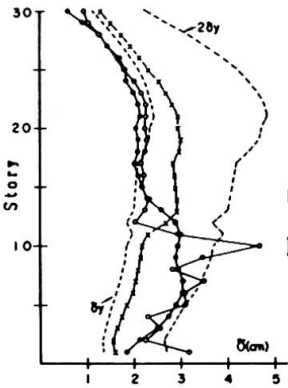

Fig. 9 Displacements between Stories Calculated by Inelastic Plane Frame Earthquake Response

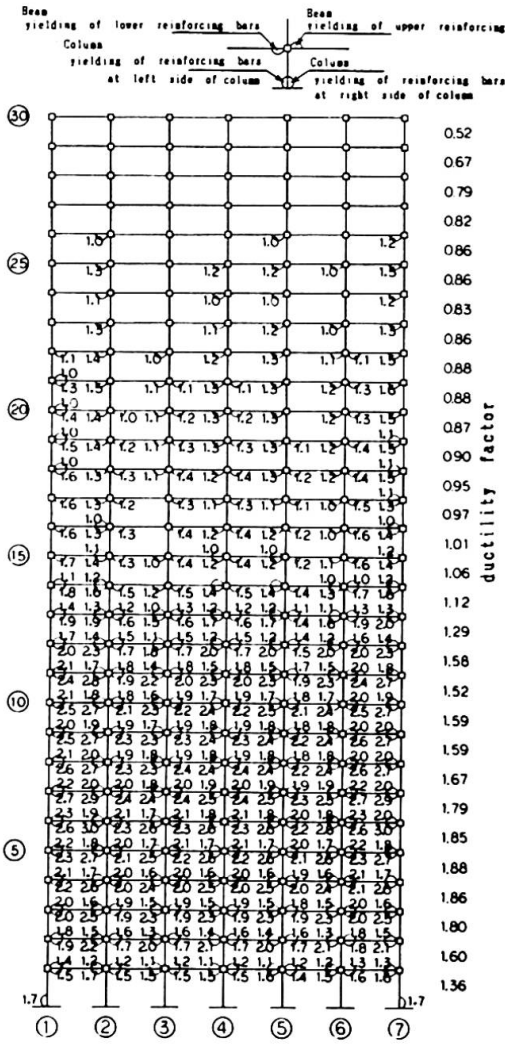

Fig.10 Yield Hinge of Beam and Column and Ductility Factor of Each Story

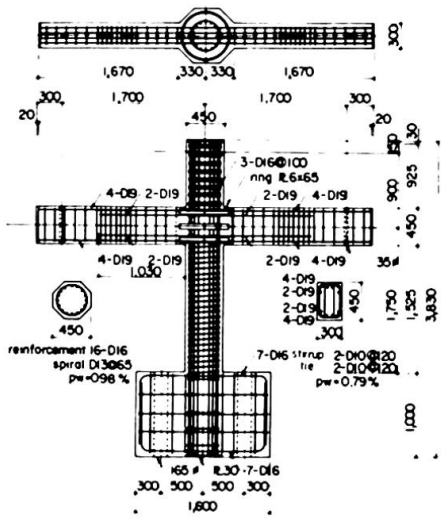

Fig.11 Specimen of Static Test

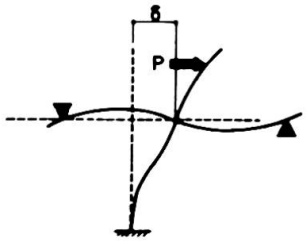

Fig.12
Loading Method and Deformation of Specimen

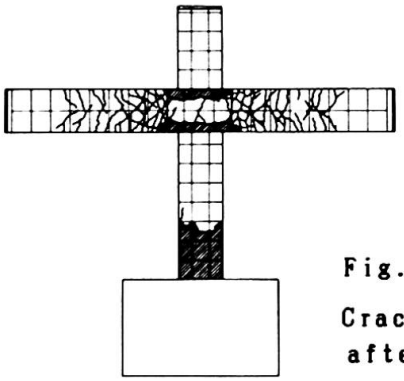

Fig.13
Cracking Pattern after Test

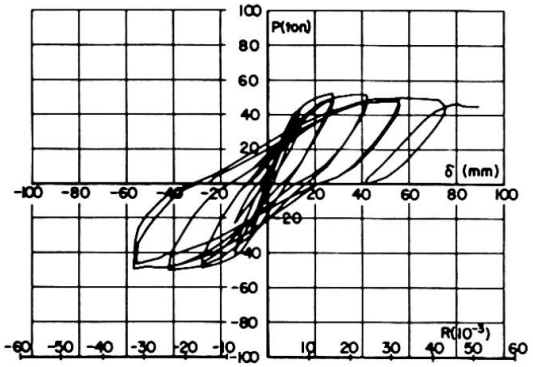

Fig.14
Load-Displacement Relationship

Table 4
Maximum Values of Measured Response

Specimen	Input Earthquake Wave	Acc (gal) Base Motion (A0)	Acc (gal) 6th Story (A6)	Disp (cm) 6th Story (Y6)	Rotational Angle (R)	Ductility Factor (μ)
YD62	HACHI/4 - 350	342 (5.162)	226 (7.528)	3.40 (9.302)	1/69	1.36
	HACHI/1 - 400	406 (18.175)	249 (18.305)	9.31 (36.875)	1/25	3.72

( ) : Occurrence Time (sec)

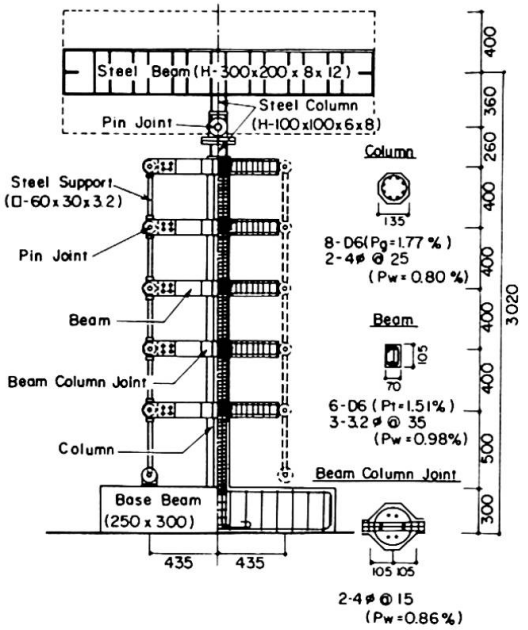

Fig.15
Specimen of Dynamic Test

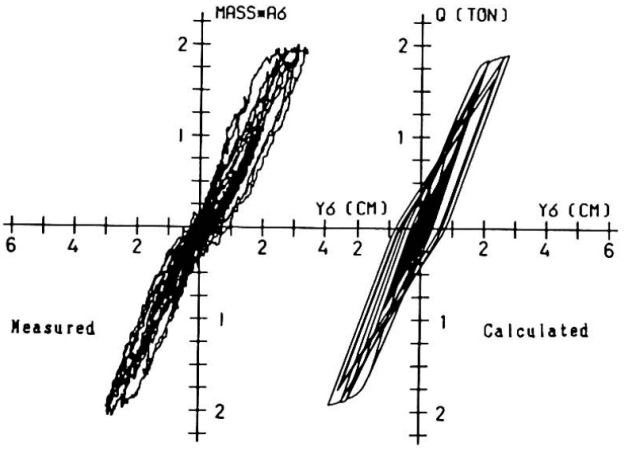

YD62,HACH1/4-350 HACH1/4-350 (ANALYSIS)

Fig.16
Force-Displacement Relationship in Test and Analysis

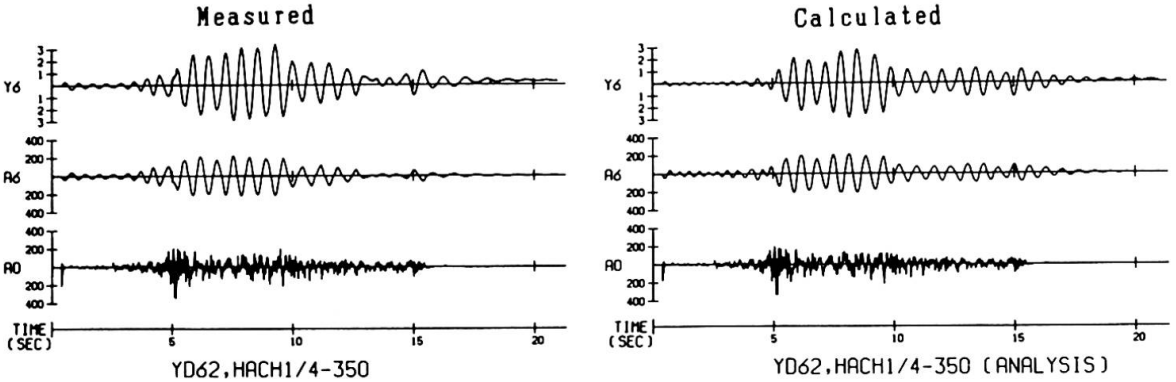

YD62,HACH1/4-350 YD62,HACH1/4-350 (ANALYSIS)

Fig.17 Time History Response in Dynamic Test and Analysis

Analysis of Space Frames under Vertical Earthquake Loads

Analyse de treillis spatiaux sous l'effet de charges sismiques verticales

Analyse von Raumfachwerken unter vertikaler Erdbebenbelastung

Yi-Gang ZHANG
Lecturer
Jilin Civil Eng. College
Changchun, China

Tien T. LAN
Senior Research Engineer
Chinese Academy of Build. Res.
Beijing, China

SUMMARY

In this paper a rational and simple method is given for estimating forces in a space frame under vertical earthquake loads. A series of commonly used space frames of different types and spans were studied by computer analysis. Results of the investigation into the free vibration characteristics and earthquake response of space frames are reported, which form the basis of the proposed method.

RESUME

Une méthode simple et rationnelle permet le calcul des forces dans un treillis spatial sous l'effet de charges sismiques verticales. Une série de treillis de types et portées différents ont été étudiés à l'aide de l'ordinateur. Les résultats de l'étude des caractéristiques des oscillations propres et le comportement aux séismes des treillis sont présentés.

ZUSAMMENFASSUNG

Es wird in dieser Arbeit ein rationales und einfaches Verfahren zur Bestimmung der Stabkräfte des Raumfachwerkes unter vertikaler Erdbebenbelastung gegeben. Eine Reihe viel verwendeter ebener Raumfachwerke verschiedenen Typs und mit verschiedenen Spannweiten wurde mit Hilfe von Computerprogrammen untersucht und studiert. Die Ergebnisse der Untersuchungen über die Charakteristiken der Eigenschwingungen und die Antwortspektren der ebenen Raumfachwerke werden aufgezeigt. Sie bilden die Grundlage für das vorgeschlagene Verfahren.

1. INTRODUCTION

Space frame has found wide applications as the roof system of buildings, especially long-span roofs. The design of steel space frame to resist earthquake loads is an urgent problem encountered to design engineers. Since the amount of work involved in the dynamic analysis of space frame is extremely large, a simple and rational method for estimating the seismic force in a space frame is required for practical design purpose. Such a method should be based on the systematic analysis of the free vibration characteristics and earthquake response of the space frame. Some design codes specify that certain magnifying factor be introduced to the static load to include the seismic effect, this seems to be irrational and does not reflect the load-resisting behavior of the structure.

On the basis of paper [1], a series of commonly used space frame supported along perimeters were studied by computer analysis and an appropriate expression for the seismic force coefficient was found. The types of the space frame are: (The names in the parenthesis indicate the terminology suggested in some English literature)

Orthogonal Type

(1) Two-way orthogonal lattice grids (Square on square)
(2) Orthogonal square pyramid space grids (Square on square offset)
(3) Orthogonal square pyramid space grids with openings (Square on larger square)
(4) Square pyramid space grids of checkerboard pattern (Square on diagonal

Diagonal Type

(5) Two-way diagonal lattice grids
(6) Diagonal square pyramid space grids (Diagonal on square)
(7) Square pyramid space grids with star elements

2. DYNAMIC BEHAVIOR OF SPACE FRAME

2.1 Free Vibration Characteristics

A space frame can be treated as a pin-connected space truss system as shown in Fig. 1. External loads are assumed to be point loads acting at the joints of top chord or bottom chord. The members resist only axial forces. The free vibration of a space frame is thus formulated as a equation of motion for a freely vibrating undamped multi-degree-of-freedom system. By solving the generalized eigenvalue problems, the circular frequencies and vibration mode vectors are obtained.

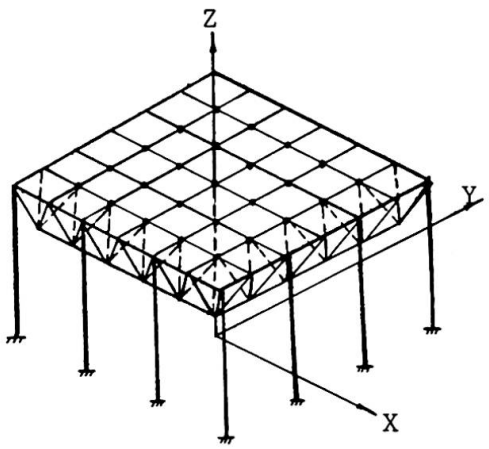

Fig. 1 Space Truss System

With each joint possessing three degrees of freedom, a space frame of ordinary size will have hundreds or thousands degrees of freedom and the amount of computing work will be tremendous. In view of the fact that only first dozens of vibration modes are needed in analysis, a sub-space iteration method is used, this results in a significant reduction of computational effort.

From paper [2], 22 space frames of different types and spans were taken for dynamic analysis. The members of the space frame were selected by optimization, so that the sectional area and static force were reasonably matching.

Calculated results show some interesting features of the free vibration charac-

teristics of the space frame. The frequency spectrums of space frames are rather concentrated and fundamental periods for most space frames range from 0.4 - 0.6 sec. and fundamental period increases with the span. It was found that the vibration modes could be classified mainly as vertical modes and horizontal modes which appear alternately. The vertical modes of different types of space frame demonstrate essentially the same shape and the vertical frequencies for different space frames of equal span are very close to each other. Certain proportion could be established between the first three frequencies of the vertical mode, which are designated as f_{v1}, f_{v2} and f_{v3} respectively, i.e.

$$f_{v2} = 3\, f_{v1} \text{ and } f_{v3} = (4 \sim 4.6)\, f_{v1}$$

2.2 Earthquake Response of Space Frame

In order to investigate the seismic behavior of space frames under vertical earthquake loads, use has been made of the following methods. First, a response spectrum method was used employing a proposed Chinese vertical spectrum [3] as shown in Fig. 2 . For comparison, a time history method was also used. The computation was implemented by Wilson-θ method employing vertical acceleration records of El Centro (1940) and Tianjin, China (1976). According to Chinese aseismic design code, the maximum vertical accelerations are 0.05g, 0.1g and 0.2g respectively corresponding to design intensities 7, 8 and 9. The peak values of the earthquake records were adjusted as the equivalents of the above design intensities.

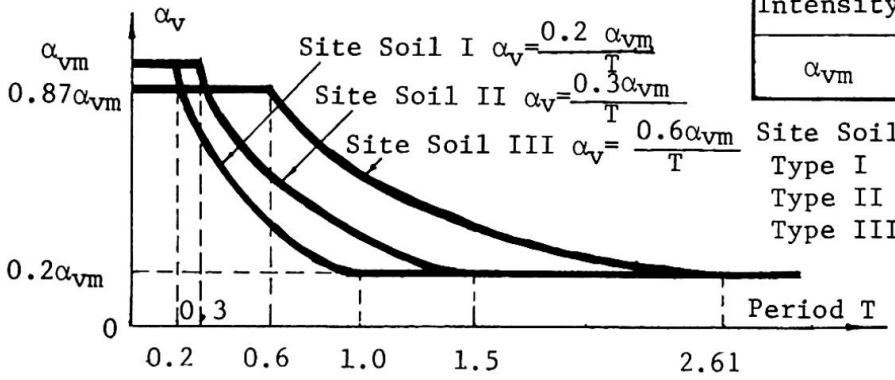

Design Intensity	7	8	9
α_{vm}	0.115	0.23	0.46

Site Soil
Type I Stable rock
Type II Ordinary stable soil
Type III Saturated loose sand, silty sand, organic soft soil etc.

α_v - Earthquake-related coefficient

Fig. 2 A Proposed Chinese Vertical Response Spectrum

It was found from the calculated results that forces in the space frame due to vertical earthquake are mainly contributed by the first three symmetrical vertical modes. Hence first ten symmetrical modes should be considered so as to include these vertical modes.

The values of vertical seismic forces in the members, whether top chords, bottom chords or webs, are higher near the central region of the space frames and decrease gradually towards the perimeters. A seismic force coefficient k_i is introduced as the ratio between the forces in ith member due to vertical earthquake and static load,

$$k_i = F_i^e \Big/ \left|F_i^s\right| \quad (i = 1,2, \ldots n) \tag{1}$$

where n is the total number of the members.

k_i values are then plotted at the midpoint of each member on the plan of space frames for different types and spans. An example is shown in Fig. 3 for a Type 1 space frame. By designating the k_i values on the symmetrical axes to scale, it can be shown that an approximately linear relation exists. Thus the

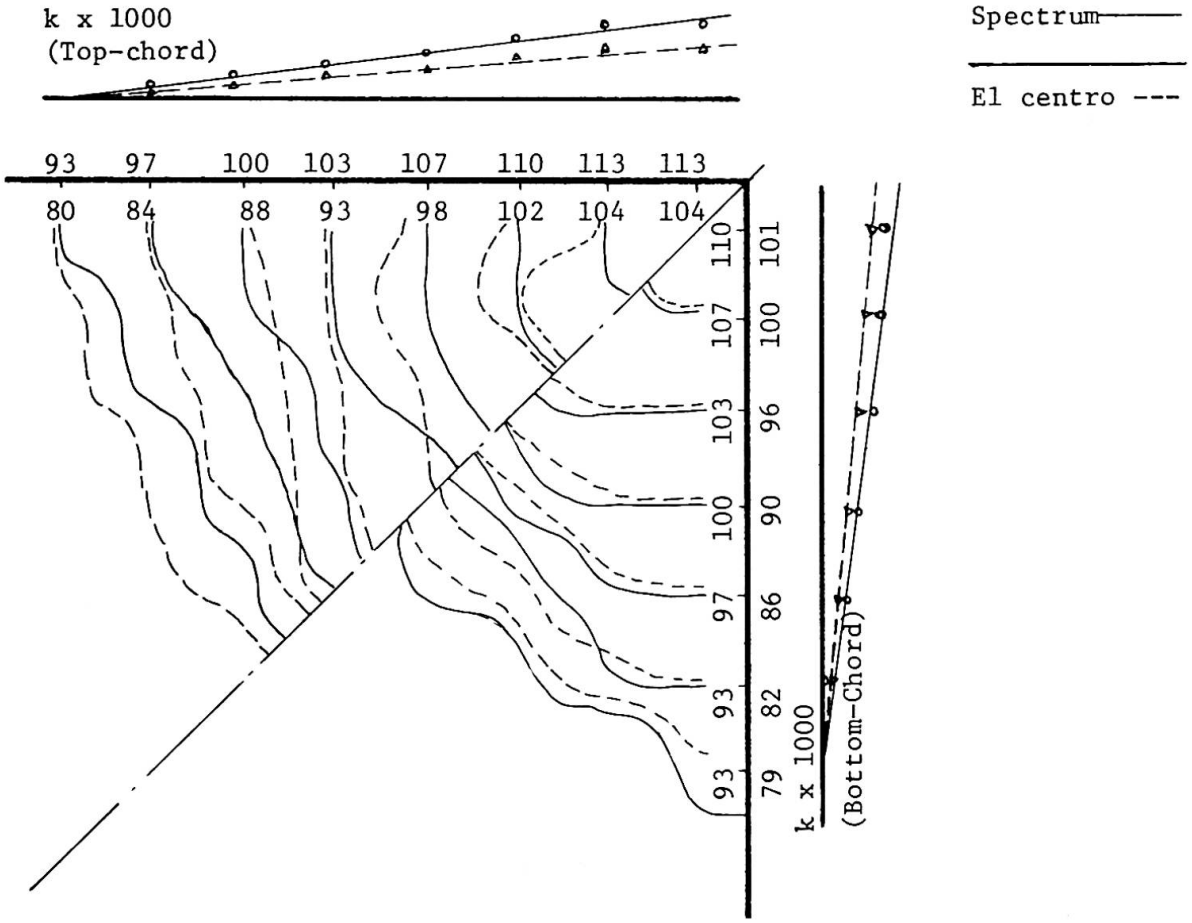

Fig. 3 Distribution of k Values in a Type 1 Space Frame (60 m x 60 m, Site Soil II, Design Intensity 8)

contour of the k_i values could be depicted in the shape of a cone as in Fig. 4 , where the top of the cone is the center of the space frame. For a rectangular plan, the base of the cone is a ellipse instead of a circle. The ordinate of the point on the surface of the cone can be taken as the k_i value for the member located at the same point. The peak value is k_{max} at center and minimum value is k_{min} along the perimeters, which are related by a reduction factor β, i.e.

$$k_{min} = \beta\, k_{max} \qquad (2)$$

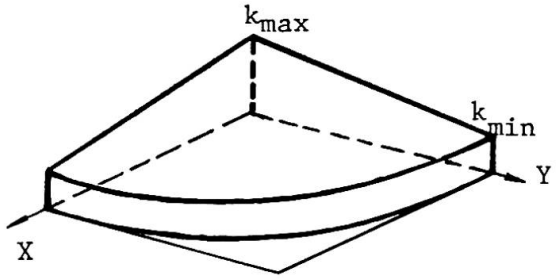

Fig. 4 Cone-shaped Distribution of Seismic Force Coefficient

3. METHOD OF ANALYSIS

In the process of space frame design, the force in each member and displacement at each node due to static loads are usually found first, therefore it is convenient to determine the force due to earthquake load on the basis of known static forces. Thus from eqation (1)

$$F_i^e = k_i \left| F_i^s \right| \quad (i = 1, 2, 3 \ldots n) \qquad (1a)$$

As shown above, the distribution of the seismic force coefficient k over the plan of a space frame is in the shape of a cone. Once the peak value k_{max} and the

reduction factor β are found, the value k_i for any member can be determined without difficulty.

After analyzing the distribution of k value of different types of space frame, it can be seen that the k values for top chord members are slightly higher than those for bottom chord members. In most cases, k values for web members near the central region of the space frame are relatively high, this is due to the fact that the sectional areas of the web members are determined by constructional requirements and are not fully-stressed as the chord members do. Therefore in determining the k_{max} and β values it is justifiable to take the top chord members to represent the whole space frame.

3.1 Peak Value of Seismic Force Coefficient

The factors influencing the seismic force in a space frame are numerous, such as the magnitude of earthquake load, the type of space frame, the grid module and depth of the space frame as well as the aspect ratio of the plan layout. Yet the only factor that can most comprehensively reflect the above parameters is the fundamental frequency of the space frame, which can express the dynamic behavior of the structure satisfactorily. Hence it is necessary to find out the relation between the peak value of seismic force coefficient k_{max} and the fundamental frequency f.

A series of space frames under various site soil conditions were analyzed and the relations between k_{max} and f are shown in Fig. 5 and 6. It was found that the seimic force of a space frame depends to a large extent on whether the layout of the top chord members is orthogonal or diagonal. The k_{max} values of the diagonal type are much higher than those of orthogonal type. It also can be seen that for different site soil, an approximately linear relation exists between k_{max} and f, and k_{max} approaches to a definite value as f increases. The above relation can be concluded as a broken line shown in Fig. 7 where the slope of the inclined section was found by regression analysis of the calculated results. It is suggested to determine k_{max} from Fig. 7 where a and b can be taken from Table 1.

For commonly used space frame in practice, the k_{max} values are usually taken from the inclined section of the broken line in Fig. 7 for type I and II site soils and from horizontal section for type III site soil. Thus the seismic force coefficient is always higher for unfavorable soil condition.

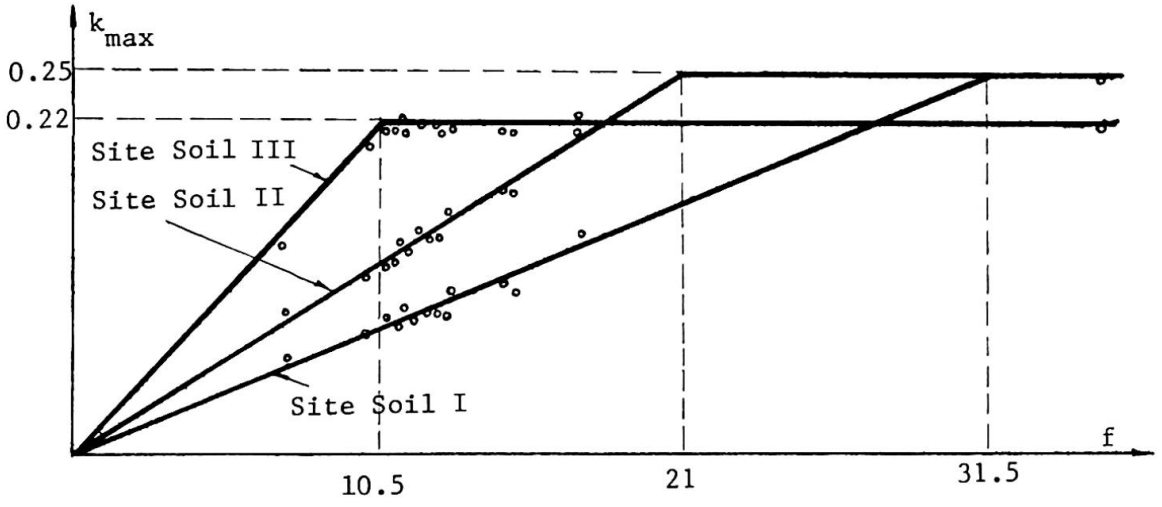

Fig. 5 k_{max} - f Relationship for Orthogonal Type Space Frame

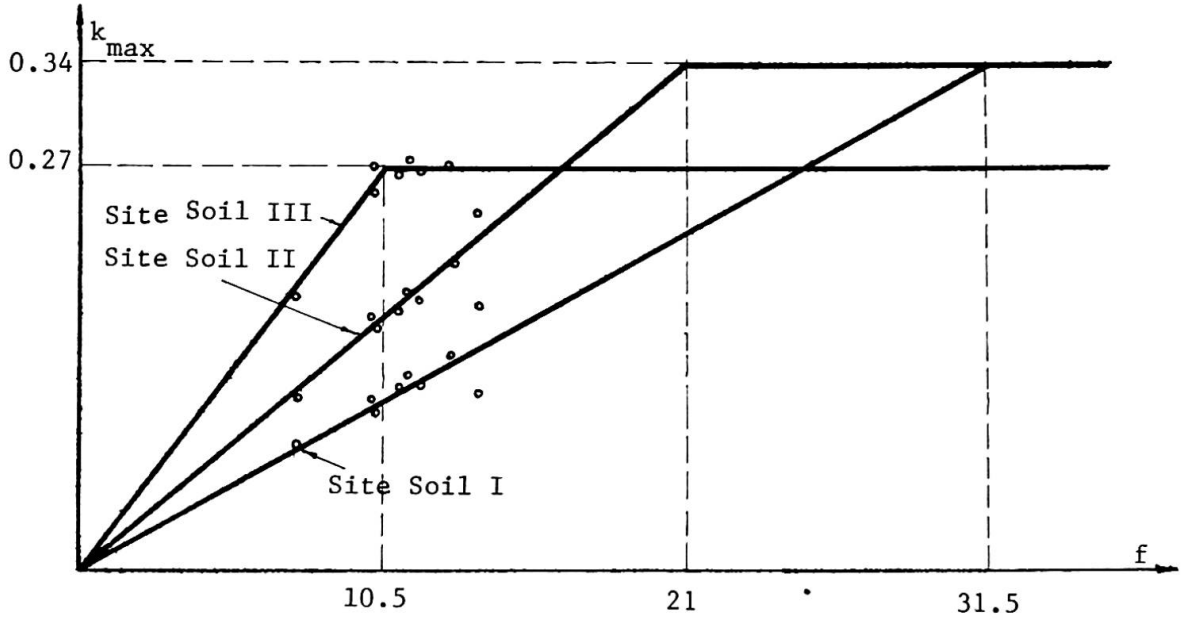

Fig. 6 k_{max} - f Relationship for Diagonal Type Space Frame

Type of Site Soil	a		b
	Orthogonal Type	Diagonal Type	
I	0.25	0.34	31.5
II			21
III	0.22	0.27	10.5

Table 1 Values of a and b in Fig. 7

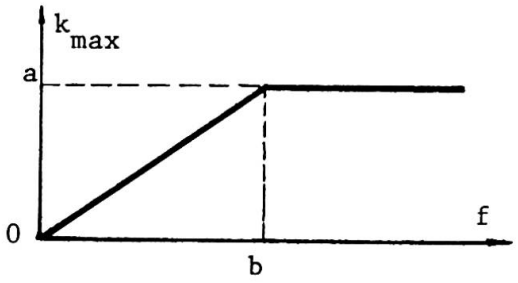

Space Frame		β
Orthogonal Type	Square	0.81
	Rectangular	0.87
Diagonal Type	Square	0.56
	Rectangular	0.80

Fig. 7 Suggested k_{max} - f Diagram Table 2 Reduction Factor β

3.2 Reduction Factor β

From the calculaed results, it can be shown that the reduction factor β is only influenced by the type and plan layout of the space frame, and irrelevant to the variation of span or type of the site soil. β value for rectangular plan is usually higher than that for square plan. It is suggested to use the β values as set forth in Table 2 which are obtained from the average values of the computed values for top chord members of various types of space frame.

3.3 Seismic Force Coefficient k_i

After determining the values k_{max} and β as mentioned above, the seismic force coefficient of any member of a space frame can be found from the following formula:

$$k_i = K\ C\ k_{max} \left[1 - \frac{L_i}{L} (1 - \beta) \right] \qquad (3)$$

where K - Coefficient considering seismic design intensity*

C - Structure-related coefficient depending on the type of structure of different constructional materials, also covering the effects of damping, ductility etc.**

L_i - Distance from the center 0 of the space frame to the midpoint of ith member

L - Length OI in Fig. 8.I is a point on the inscribed ellipse (or circle) of the plan

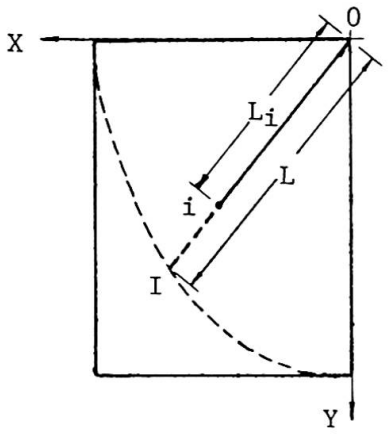

Fig. 8 Plan of a Space Frame

3.4 Method for Calculating Fundamental Frequency f

In order to determine k_{max} it is necessary to get the fundamental frequency f of the space frame first, which can be obtained from dynamic analysis or testing result. In practical engineering design, energy method could be used to calculate the fundamental frequency, using the curved surface of the vertical displacements under static loads as an approximation of the first vibration mode. Thus, the formula for calculating fundamental frequency can be written as:

$$f = \sqrt{g \frac{\sum_{k=1}^{N} W_k Z_k}{\sum_{k=1}^{N} W_k Z_k^2}} \qquad (4)$$

where W_k is the static load at kth node point, Z_k is the vertical displacement under static load at kth node point and N is the total number of node points. As can be seen from Table 3, this method is efficient for obtaining relatively accurate values of fundamental frequency of different types of space frame.

---

* According to Chinese aseismic design code, for design intensities 7, 8 and 9 the K values are taken as 0.5, 1 and 2 respectively.

**C value is essentially emperical, it is suggested to be 0.35 for steel space frame.

Space Frame		Fundamental Frequency	
Type	Size in m	Accurate Analysis	Approximate Value fr.eq.(4)
1	24 x 36	16.643	16.966
2	48 x 48	12.324	12.547
3	48 x 48	10.920	11.109
4	36 x 36	16.410	16.671
5	50.4 x 61.6	10.267	10.544
6	60 x 60	10.396	10.627
7	48 x 48	11.791	12.024

Table 3 Comparison of Accurate and Approximate Values of f

4. CONCLUSION

By means of the computer analysis of a series of space frames of different types and spans, the free vibration characteristics and the pattern of the internal forces in the space frame due to vertical earthquake are basically clarified. A practical method of design is given. For any space frame, once the fundamental frequency is known, the peak value k_{max} of seismic force coefficient and the reduction factor β are easily determined. Then the seismic force in any member of the space frame can be calculated by formula (1a), which is simply the product of the seismic force coefficient and the force due to static load. The infuluences due to the type of space frames and their site soil conditions as well as the variation in the dynamic behavior of the space frame are all included in the proposed method so that a more rational estimation of seismic forces can be obtained as compared to current practice.

REFERENCES

1. ZHANG Y., Optimum Aseismic Design with Finite Element Method for Double Layer Grid Truss. Proceedings of the International Conference on Finite Element Methods. Science Press, Beijing, China, 1982.

2. LAN T., Yu J.L., QIAN R.J., A Study on the Optimum Design of Space Trusses - Optimal Geometrical Configuration and Selection of Type. Selected Papers on Space Structures, Science Press, Beijing, China, 1984. (in Chinese)

3. SHE S.H. Vertical Earthquake Spectrum, Journal of Harbin Civil Engineering Institute, No. 2, 1982. (In Chinese)

4. Aseismic Design Code for Industrial and Civil Buildings (TJ 11-78), China Constructional Industry Press, Beijing, China, 1979.

Ultimate State Aseismic Design of Reinforced Concrete Structures

Calcul à l'état limite de ruine des structures en béton armé sous l'effet de séismes

Grenztragfähigkeit von Stahlbeton unter Erdbebenbelastung

Minoru YAMADA
Prof. Dr.-Eng.
Kobe Univ.
Kobe, Japan

Minoru Yamada, born 1930, received his doctor degree 1959 from the Kyoto University, Japan. His research findings on the shear explosion effect in short reinforced concrete columns was later verified in the Tokachi-Oki earthquake in 1968. He has been professor of structural engineering, Kobe University, Japan, since 1964.

SUMMARY

The practical dimensioning formulae, not only for strength but also for deformation, for the ultimate state aseismic design of reinforced concrete structures are presented here not empirically but analytically, based upon the fundamental mechanical properties of materials. Using these formulae it is possible to estimate quantitatively the ultimate aseismic capacity of reinforced concrete structures.

RESUME

L'article présente des formules pratiques de calcul à la rupture de structures en béton armé, sous l'effet de séismes. Ces formules, tenant compte de la résistance et des déformations, sont basées sur les propriétés mécaniques fondamentales des matériaux. L'application de ces formules permet de quantifier la sécurité des structures en béton armé, vis à vis de tremblements de terre.

ZUSAMMENFASSUNG

Analytisch hergeleitete Bemessungsformeln für Stahlbetonbauten unter Erdbebenbelastung werden vorgeschlagen. Sie basieren auf den mechanischen Eigenschaften der beiden Komponenten Stahl und Beton und berücksichtigen auch die Verformungen. Mit diesen Bemessungsformeln wird es möglich, die Grenztragfähigkeit von Stahlbeton unter Erdbebenbelastung quantitativ abzuschätzen.

1. INTRODUCTION

The importances of the ultimate state design of reinforced concrete structures for earthquakes were already principally well recognized. However, the lack of practical dimensioning formulae [1] especially the lack of analytical evaluation formulae of plastic deformations or deterioration and fracture processes makes the practical application of ultimate state aseismic design impossible. It is proposed here from this point of view the dimensioning formulae of reinforced concrete aseismic elements not only ultimate resistances but also ultimate deformation based upon only characteristic mechanical values of materials, i.e. concrete and steel, not empirically but analytically.

2. ASEISMIC ELEMENTS OF REINFORCED CONCRETE STRUCTURES

2.1 Classification of Reinforced Concrete Aseismic Elements

Reinforced concrete structures are consisted of the following five aseismic elements:

1) Reinforced Concrete Short Columns (SC), with a shear span ratio (H/D) shorter than 4, predominant of the influences of shear forces (V) than bending moment (M) and axial load (N), show explosive shear fracture at a very small relative displacements without ductility.
2) Reinforced Concrete Medium Columns (MC), with a shear span ratio (H/D) between 4 to 20, predominant of the influences of bending moment (M) than shear force (V) and axial load (N), show bending yield at a fairly large relative displacement with some or sufficient ductility.
3) Reinforced Concrete Long Columns (LC), with a shear span ratio (H/D) larger than 20, predominant of the influences of axial load (N) than bending moment (M) and shear force (V).
4) Reinforced Concrete Shear Walls (SW), show large resistances but without ductility.
5) Reinforced Concrete Shear Walls with Openings (SWO), show medium resistance between shear wall without openings and rigid frames.

Under one way sway loading, like earthquake, these aseismic elements show quite different resisting and deformation behaviours of each other, such as shown in Fig. 1, under the fixed constraint of top and bottom ends.

2.2 Importances of the Differences of Deformability of Reinforced Concrete Elements

Because of the high rigidity of so-called " Scheibe-action " of floors, each aseismic elements are constrained to remove the same relative displacement between floors. Therefore the large differences of deformability of each aseismic elements hold no more the simple superposition principle of ultimate resistances of elements and cause the elasto-plastic deformation and fracture

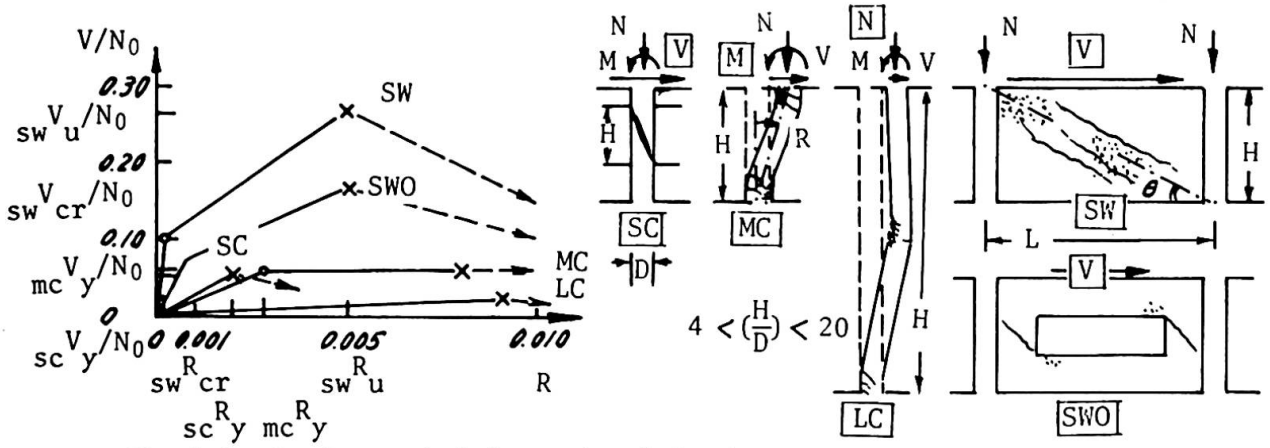

Fig.1 Resisting and deformation behaviours of aseismic elements

behaviours of whole structures very complex. The resistances of each elements are only able to superposed at the same values of displacements. Thus caused the whole resisting behaviour and fracture of reinforced concrete buildings [2] by the drastic reduction [1] of bearing capacity and ductility of short columns.

In this report a reinforced concrete cross section is abstracted into a poly-mass points-model such as shown in Fig.2(a) and the characteristic values of materials (concrete and steel) are illustrated in Fig.2(b) for analysis. (see Fig.2)

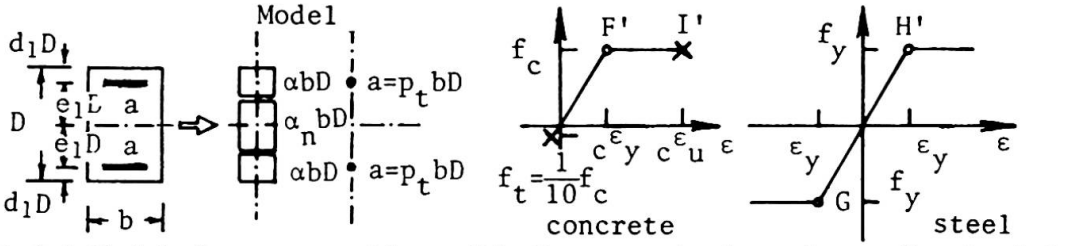

Fig.2 (a) Modeled cross section (b) Characteristic values of materials

3. REINFORCED CONCRETE SHORT COLUMNS

3.1 One Way Sway Loading

Reinforced concrete short columns with a smaller shear span ratio (H/D) than 4, are predominated shear behaviour than bending and normal forces, and show violent shear explosion [2] at a shear resistance V_y^s with a very small relative sway displacement angle R_y^s or displacement δ_y^s between stories as follows [3][4].

$$V_y^s = \tau_y A_{se} = \frac{7}{8}(1-d_1) f_c bD\sqrt{-0,10(X)^2+0,09(X)+0,01} \quad (1),$$

$$R_y^s = {}_c\gamma_y = \tau_y/G_c = f_c\sqrt{-0,10(X)^2+0,09(X)+0,01}/G_c \quad (2),$$

$$\delta_y^s = R_y^s H \quad (3),$$

where

$A_{se} = \frac{7}{8}(1-d_1)bD$: effective cross sectional area for shear,

$X = N/N_0$: axial load level ratio,

$N_0 = f_c bD\{1+2(f_y/f_c)p_t\}$: ultimate strength of centrally loaded columns, (4),

$G_c = \tau_y/{}_c\gamma_y = 0,9\times10^5 kg/cm^2$: shear modulus of concrete. (see Fig.3)

Fracture condition of concrete under the combined stresses of σ and τ are assumed to be:

$$\tau_y/f_c = \sqrt{-0,10(\sigma/f_c)^2+0,09(\sigma/f_c)+0,01}.$$

Ductility of reinforced concrete short columns may only be expected with a very sufficient hoop reinforcement p_w more than 1% or more. (see Fig.3)

3.2 Cyclic Sway Loading

Under cyclic sway loading, reinforced concrete short columns show a drastic reduction of resistances and deformation capacities. Therefore, it is unable to expect any resistances of such reinforced concrete short columns under cyclic sway loadings.

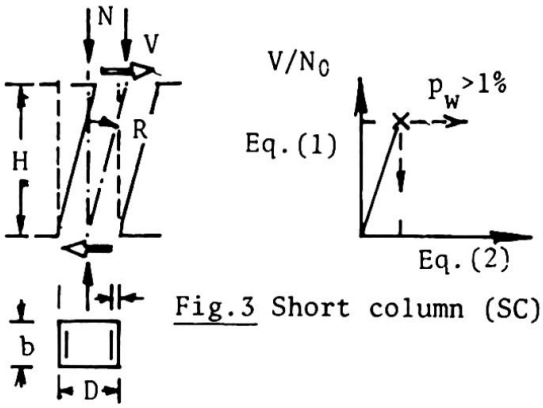

Fig.3 Short column (SC)

4. REINFORCED CONCRETE MEDIUM COLUMNS

4.1 One Way Sway Loading

Reinforced concrete medium length columns with a shear span ratio (H/D) between 4 to 20 are predominated by the influences of bending moment M than shear V and axial force N.

Story yield shear force V_y^B and story yield sway displacement δ_y^B under bending yield of both (top and bottom) fixed ends of medium length columns are:

$$V_y^B = 2M_y/H \quad (5),$$

$$\delta_y^B = (H^2/6)\Phi \quad (6),$$

where

(a) for lower axial load level: $0 \leqq X \leqq \dfrac{\alpha}{1+2(f_y/f_c)p_t}$

$$M_y = f_c bD^2\{N/f_c bD+2(f_y/f_c)p_t\}e_1 \quad (7),$$

$$\Phi_y = -\frac{\varepsilon_y}{2e_1 D}\left\{\frac{N/f_c bD+(f_y/f_c)p_t}{\alpha+(f_y/f_c)p_t}+1\right\} \quad (8).$$

(b) for higher axial load level: $\dfrac{\alpha}{1+2(f_y/f_c)p_t} \leqq X \leqq \dfrac{\alpha+(3/4)\alpha_n}{1+2(f_y/f_c)p_t}$

$$M_y = f_c bD^2\left\{2-\frac{N/f_c bD}{\alpha+(3/4)\alpha_n}\right\}\{\alpha+(f_y/f_c)p_t\}e_1 \quad (9),$$

$$\Phi_y = -\frac{\varepsilon_y}{2e_1 D}\left\{\frac{N/f_c bD}{\alpha+(3/4)\alpha_n}-2\right\} \quad (10),$$

where

$$2\alpha+\alpha_n = 1 \text{ (cf.Fig.2)(see Fig.4(a))} \quad (11).$$

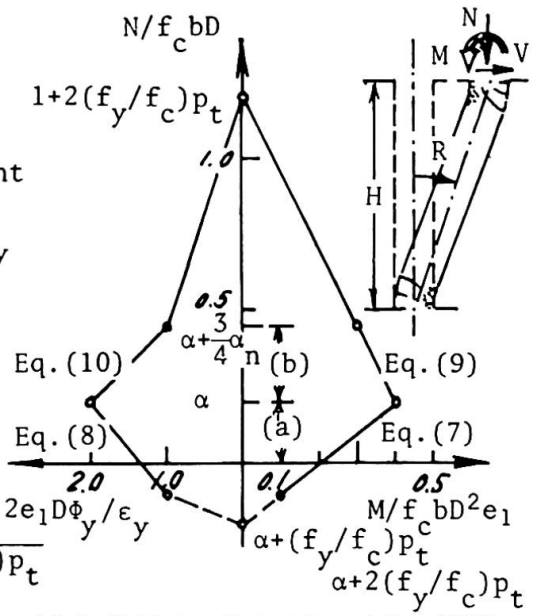

Fig.4(a) N-M-Φ_y-Relationship (MC)

4.2 Cyclic Sway Loading

For only the cases of constant curvature amplitude and tensile yield $\left(0 \leqq \dfrac{N}{f_c bD} \leqq \alpha\right)$ Under the assumption of the formation of cyclic plastic hinge zones with a hinge length of λD (λ=1) at the both (top and bottom) fixed ends of columns, then story yield shear force V_y^B, story slip shear force V_s^B, and story yield sway displacement δ_y^B, story sway displacement amplitude δ_a under bending yield are:

$$V_y^B = \frac{2M_y}{H}, \quad V_s^B = \frac{2M_s}{H} \quad (12),$$

$$\delta_y^B = \frac{H^2}{6}\Phi_y, \quad \delta_a = \delta_y+\lambda D(\Phi_a-\Phi_y)H \quad (13),$$

where

$$M_y = f_c bD^2\left\{\frac{N}{f_c bD}+2(f_y/f_c)p_t\right\}e_1 \quad (14),$$

$$M_s = f_c bD^2\left\{2(f_y/f_c)p_t-\frac{N}{f_c bD}\right\}e_1 \quad (15),$$

$$\Phi_y = \frac{2e_1 D}{\varepsilon_y} = 2 \quad (16).$$

see Fig.4(b).

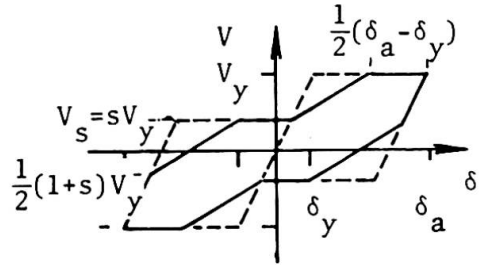

Fig.4(b) Hysteresis loop of medium column

4.3 Ductility Factor

Plastic hinges of reinforced concrete medium columns are formed only by the tensile yielding of longitudinal reinforcement at G and the rotation capacity of them are limited by the reach of concrete strains to the ultimate value ${}_c\varepsilon_u = 0{,}004$ (ultimate compressive strain of concrete at I').

The ductility factor μ of reinforced concrete medium columns under one way sway are:

$$\mu = \frac{\Phi_u}{\Phi_y} = \frac{1}{n_1}\left(\frac{{}_c\varepsilon_u}{\varepsilon_y} - \frac{1}{2}\right)\frac{2}{3}(1 - d_1 - n_1) \geq 1 \qquad (17),$$

see Figs.5,6.

From Eq.(17) the plastic hinges are formed only under the lower axial load level than the intersection point of G and I' so,

$$n_1 = 0{,}53 \qquad (18).$$

The ductility factor μ of reinforced concrete medium columns under cyclic sway are computed under the assumption of the reduction γ of concrete resistances by the repetition number of loadings N such as shown in Fig.7, and the fatigue fracture occures by reach of the compressive strain of concrete at the compressive longitudinal reinforcement to the compressive ultimate strain ${}_c\varepsilon_u$, then the relationship between curvature amplitude Φ_a and number of cycles until fracture becomes

$$\Phi_a = \frac{1}{D}\,\frac{{}_c\varepsilon_u}{\dfrac{1}{1 - \frac{1}{8}\log_{10} N_B}\,\dfrac{N}{f_c bD} - d_1} \qquad (19).$$

For the axial load level the relationship is illustrated in Fig.8, in which the the values at $N_B = 10^0 (= 1)$ approximately corresponding to the values at $N/f_c bD = 0{,}2$ in Fig.5.

The relationships between the ductility factor μ and the number of cycles to fracture N_B are (see Fig.9),

$$\mu = 1 + \{\lambda D(\Phi_a - \Phi_y)H\}/\delta_y \qquad (20).$$

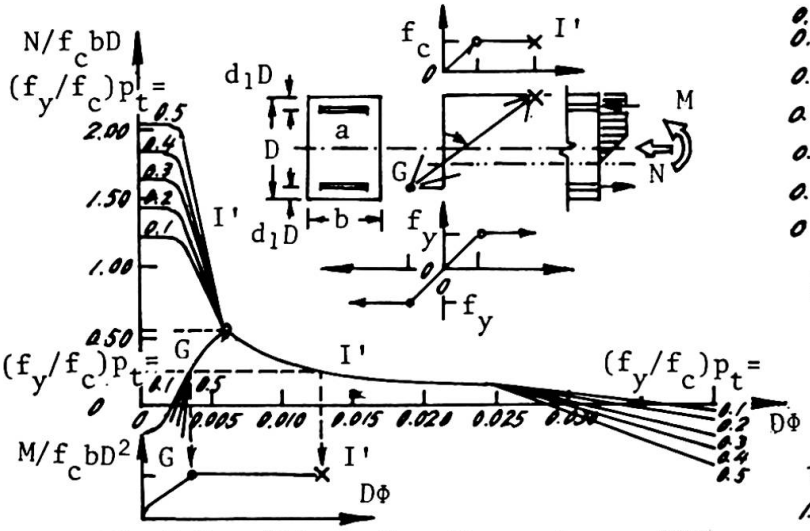

Fig.5 Ductility of medium columns (MC)

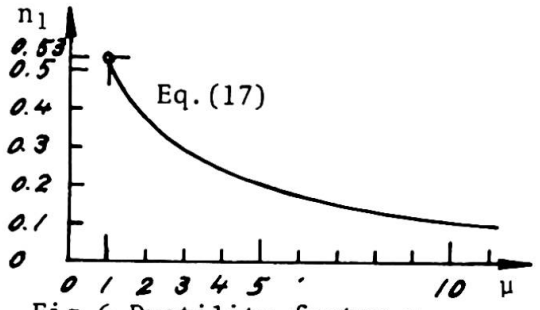

Fig.6 Ductility factor μ

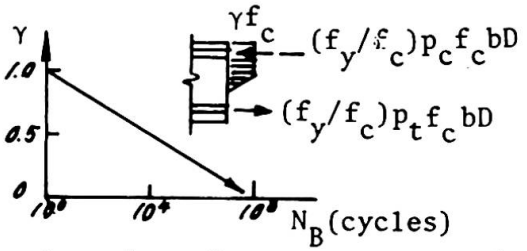

Fig.7 Deterioration of concrete strength

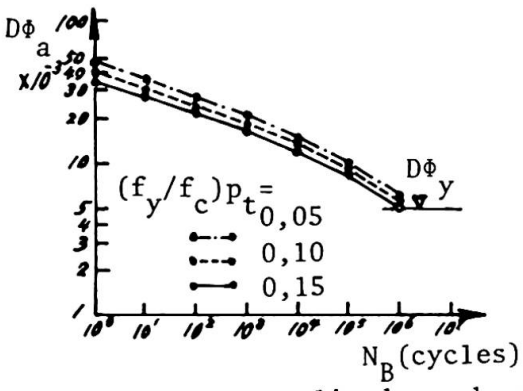

Fig.8 Curvature amplitude-number of cycles to fracture

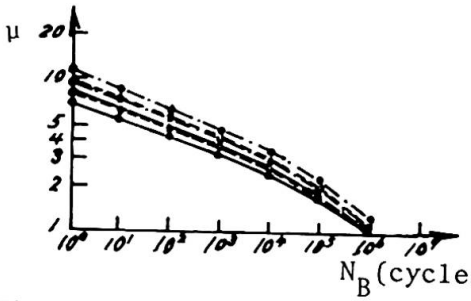

Fig.9 Ductility factor-number of cycles to fracture

5. REINFORCED CONCRETE LONG COLUMNS

5.1 One Way Sway Loading

One way sway loading of reinforced concrete long columns show unstable states. The ultimate N-M-Interaction curves indicate the influences of the values of shear span ratios (H/D) (see Fig.10). So there exist no ductility in long columns with larger shear span ratios (H/D) > 20.

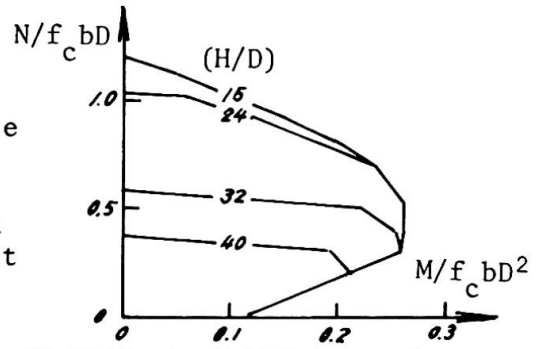

Fig.10 Ultimate N-M-Interaction curve of long columns (LC)

6. CRITICAL SHEAR SPAN RATIOS

There exist two critical shear span ratios of reinforced concrete columns, i.e. between short columns (SC) with shear explosion and medium column (MC) with bending yield $(H/D)^{I}_{cr}$; and between medium column (MC) with bending yield and long column (LC) with buckling $(H/D)^{II}_{cr}$.

6.1 Critical Shear Span Ratio $(H/D)^{I}_{cr}$

The critical shear span ratio $(H/D)^{I}_{cr}$ is characterized by the intersecting condition of bending yield of (MC) and shear explosion of (SC) [2][4] as follows: (Fig.11)

(a) for lower axial load level: $0 \leq X \leq \dfrac{\alpha}{1+2(f_y/f_c)p_t}$

$$(H/D)^{I}_{cr} = \frac{2\{X+2(1+X)(f_y/f_c)p_t\}\{(1/2)-d_1\}}{(7/8)(1-d_1)\sqrt{-0,10X^2+0,09X+0,01}} \quad (21),$$

(b) for medium axial load level:

$$\frac{\alpha}{1+2(f_y/f_c)p_t} \leq X \leq \frac{\alpha+(3/4)\alpha_n}{1+2(f_y/f_c)p_t}$$

$$(H/D)^{I}_{cr} = \frac{2\{\alpha+(f_y/f_c)p_t\}\{(1/2)-d_1\}}{(7/8)(1-d_1)\sqrt{-0,10X^2+0,09X+0,01}} \quad (22),$$

then

$$N = XN = 0,53 f_c bD \quad (23).$$

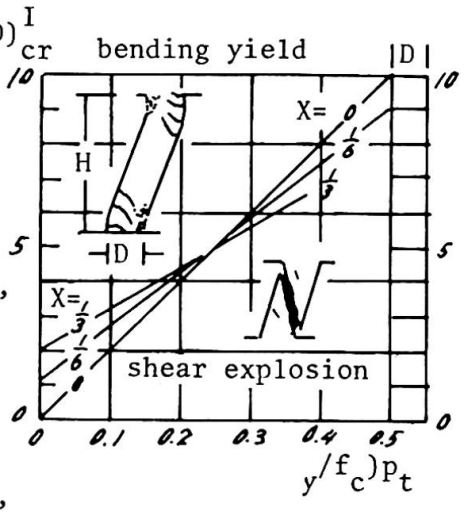

Fig.11 Critical shear span ratio $(H/D)^{I}_{cr}$

6.2 Critical Shear Span Ratio $(H/D)^{II}_{cr}$

The critical shear span ratio $(H/D)^{II}_{cr}$ is characterized by the buckling of long columns. The analytical results of ultimate N-M-Interaction curves in Fig.10 show unstable states occurres under longer columns $(H/D)_{cr} > 20$. For double curvature critical shear span ratio $(H/D)^{II}_{cr}$ varies with the axial load levels X too.

7. REINFORCED CONCRETE INFILLED SHEAR WALLS

The resisting mechanismus of reinforced concrete infilled shear walls against horizontal shear load like earthquake excitation are abstracted into a compression bracing field by concrete [5] such as shown in Fig.12.

7.1 Initial Cracking Load and Cracking Sway Displacement

Initial cracking shear force V_{cr} and relative story sway angle R_{cr} are under the assumption of uniform distribution of shearing stresses in web panel of wall with a thickness of t:

$$V_{cr} = \tau_{cr} Lt = \frac{f_c}{10} Lt \ (=0,1 f_c Lt) \quad (24),$$

$$R_{cr} = \frac{\tau_{cr}}{G_c} = \frac{f_c}{10}\frac{1}{G_c} = \frac{2(1+\nu)}{E_c}\frac{f_c}{10} \ (= 0,000001166\ f_c) \quad (25).$$

7.2 Ultimate Resistance V_u and Fracture Sway Displacement R_u

Ultimate reisistance and fracture sway displacement are under the assumption of the formation of concrete bracing:

$$V_u = f_c B_e t \cos\theta = \frac{2}{3} f_c Lt \sin\theta\cos\theta \quad (26),$$

$$R_u = \frac{c\varepsilon_u}{\sin\theta\ \cos\theta} = \frac{0,002}{\sin\theta\ \cos\theta} \quad (27),$$

see Fig.12.

7.3 Cyclic Sway Loading

Under cyclic sway loading infilled shear walls show their resistances only at the verginal part so the resistances and displacements under cyclic sway loading are abstracted into a fragmental pair resistances until ultimate resistances [7][8] such as shown in Fig.13.

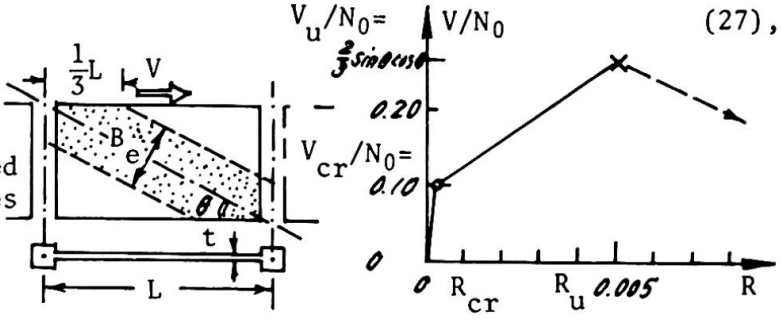

Fig.12 Shear walls (SW)

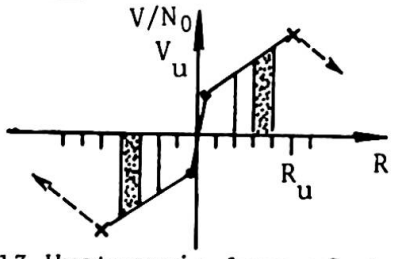

Fig.13 Hysteresis loop of shear wall

8. REINFORCED CONCRETE INFILLED SHEAR WALLS WITH OPENINGS

The resisting mechanismus of reinforced concrete infilled shear walls with openings against horizontal shear load are very complicated by the differences of fracture processes according to the different sizes and positions of openings in walls [6]. Their load-deformation relationships are situated between shear walls without openings and surrounding rigid frames such as illustrated in Fig.1. Analytical evaluation of resistances and deformations for such shear walls with openings are only possible in the cases of symmetric single openings in walls with opening width ratio $l_1=L_0/L_i$, and depth ratio $h_1=H_0/H_i$ [6] in Fig. 14.

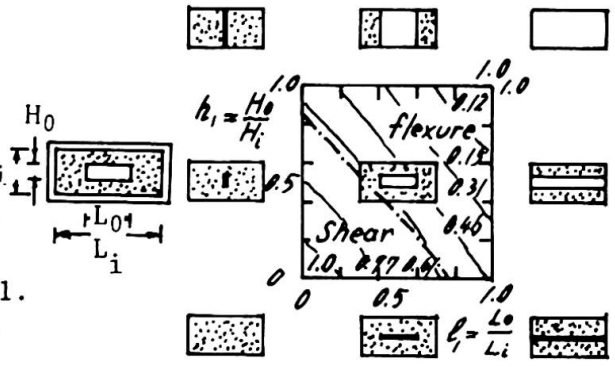

Fig.14 Ultimate resistances of shear walls with openings [6]

9. CONCLUDING REMARKS

Resisting elements of reinforced concrete structures against horizontal load like earthquake excitation are classified into short columns (SC), medium columns (MC) long columns (LC), shear walls without openings (SW) and shear walls with openings (SWO). The analytical formulae of their ultimate resistances as well as ultimate deformations, and critical shear span ratios are presented here based only upon the fundamental mechanical characteristic values of elemental materials (concrete and steel).

REFERENCES

1. TASSIOS T. P., Structural Engineering in Earthquake Zones. Introd. Rep. 12th. Congr., IABSE, Vancouver, Sep. 1984, pp.25-34.

2. YAMADA M., FURUI S., Shear Resistance and Explosive Cleavage Failure of Reinforced Concrete Members Subjected to Axial Load. Finl. Rep. 8th. Congr., IABSE New York, Sep. 1984, pp.1091-1102.

3. YAMADA M., Shear Strength, Deformation and Explosion of Reinforced Concrete Short Columns. ACI SP-42, Shear in Reinforced Concrete, Vol.2, 1974,pp.617-638

4. YAMADA M., KAWAMURA H. , Simplified Calculation Method for Flexural and Shear Strength and Deformation of Reinforced Concrete Columns under Constant Axial Loads. Rep., Working. Comm., IABSE, Vol.16, Symp., Quebec, 1974, pp.153-160.

5. YAMADA M., KAWAMURA H., KATAGIHARA K., Reinforced Concrete Shear Walls Without Openings, Tests and Analysis, ACI SP-42, Shear in Reinforced Concrete, Vol.2, 1974, pp. 539-558.

6. YAMADA M., KAWAMURA H., KATAGIHARA K., Reinforced Concrete Shear Walls With Openings, Tests and Analysis, ACI SP-42, Shear in Reinforced Concrete, Vol.2, 1974, pp. 559-578.

7. YAMADA M., KAWAMURA H., KATAGIHARA K., MORITAKA H., Cyclic Deformation Behaviour of Reinforced Concrete Shear Walls, Proc., 6 WCEE, New Delhi, 1977,Vol.III pp.

8. YAMADA M., KAWAMURA H., Ultimate Aseismic Safety of Reinforced Concrete Structures, Proc., 7 WCEE, Istanbul, 1980, Vol.4, pp.351-358.

Steifigkeits- und Dämpfungsänderung in Stahlbetontragwerken bei Erdbeben

Stiffness and Damping Changes in Reinforced Concrete Structures during Earthquakes

Effet d'un séisme sur la rigidité et l'amortissement d'une structure en béton armé

Gert KÖNIG
Professor Dr.-Ing.
TH Darmstadt
Fed. Rep. of Germany

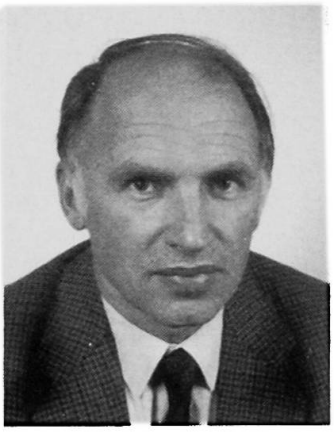

Geboren 1934. Studium des Bauingenieurwesens an der Technischen Hochschule Darmstadt, 1960 Diplom. Seit 1971 Beratender Ingenieur VBI, seit 1972 Prüfingenieur für Baustatik. 1975 Berufung an die Technische Hochschule Darmstadt. Arbeitsgebiete: Spannbetonbrücken, Hochhäuser aus Stahlbeton, Kernkraftwerke, Baudynamik, Grundlagen des Massivbaus.

Atilla ÖTES
Dipl.-Ing.
TH Darmstadt
Fed. Rep. of Germany

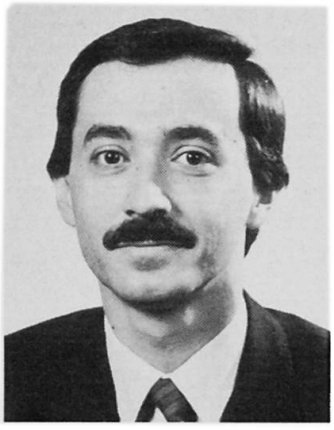

Geboren 1953. Studium des Bauingenieurwesens an der Technischen Hochschule Darmstadt, 1977 Diplom, Tätigkeit in einem Ingenieurbüro. Seit 1980 am Institut für Massivbau TH Darmstadt als wissenschaftlicher Assistent auf dem Gebiet der Erdbebenbeanspruchung von Stahlbetontragwerken tätig.

ZUSAMMENFASSUNG

Zur realistischen Beurteilung von Beanspruchungen in Stahlbetontragwerken beim Lastfall Erdbeben ist u.a. die Kenntnis über die Änderung der Steifigkeits- und Dämpfungseigenschaften des Tragwerks erforderlich. Der Aufsatz interpretiert Erdbebensimulationsversuche an Rahmenbauteilen und stellt zwei Modelle vor: Ein werkstoffgerechtes Modell zwecks genauerer Tragwerksanalyse und ein einfaches Näherungsmodell zum überschläglichen Nachweis der Tragfähigkeit.

SUMMARY

For a realistic assessment of seismic loads in reinforced concrete structures a knowledge of the stiffness and damping characteristics is essential. The paper interprets earthquake simulation tests on members of reinforced concrete frame structures and makes two alternative suggestions for modelling: A model based on material properties and developed for accurate analysis of frames and a simple, practical model for a rough check of the load carrying capacity.

RESUME

Pour juger de façon réaliste les sollicitations des structures en béton armé lors d'un séisme, il faut connaître les modifications des rigidités et des propriétés d'amortissement. Cette contribution interprète des essais de simulation sur des cadres et présente deux modèles: un modèle plus complet qui tient compte des propriétés des matériaux et un modèle plus simple pour une estimation de la capacité portante.

1. EINFÜHRUNG

Die Erdbebentauglichkeit von Rahmentragwerken aus Stahlbeton wurde in den letzten zwei Jahrzehnten erheblich erhöht. Das dabei verfolgte Prinzip, zähes Bauteilverhalten mit guten dissipativen Eigenschaften zu bewerkstelligen, ist ein optimales Konstruktionskonzept für einen Lastfall, dem wegen der geringen Auftretenshäufigkeit wirtschaftlich begegnet werden soll. [1]

Möglichkeiten für große Verformbarkeit ohne Versagen (Duktilität) bietet beim Stahlbeton die Werkstoffkomponente Stahl. Durch eine entsprechende Proportionierung der zähen, plastifizierbaren Komponente (Stahl) und der eher spröden Komponente (Beton) in den Riegeln und Stielen eines Rahmentragwerkes können hohe zyklische Beanspruchungen durch z.T. plastische Verformungen aufgenommen werden, ohne daß große Schnittgrößen entstehen müssen. [2]

Für den Ingenieur, der die Trag- und Gebrauchsfähigkeit des Tragwerks unter Berücksichtigung von Wirtschaftlichkeitsaspekten sicherstellen soll, hat das Prinzip duktilen Konstruierens die Konsequenz, daß er sich mit nichtlinearem und plastischem Bauteilverhalten auseinandersetzen muß. Weil das Materialverhalten die Übertragung der dynamischen Anregung vom Baugrund auf die einzelnen Tragwerksmassen mitgestaltet, entscheidet es im zeitlichen Ablauf auch stets darüber, wie groß die vom Bauwerk absorbierte Energie bzw. die tatsächliche Beanspruchung im Tragwerk wird.

So werden neben dem ersten Schritt der dynamischen Berechnung, nämlich der diskreten Abbildung des Bauwerks in ein mechanisches Tragwerksmodell mit Steifigkeiten und Massen, nun auch realistische Rechenmodelle benötigt, die die Steifigkeits- und Dämpfungseigenschaften wirklichkeitsnah erfassen.

Unterscheidet man dabei zwischen der Bemessungsaufgabe und der Nachweisaufgabe, die der Ingenieur zu bewältigen hat, so soll dafür gesorgt werden, daß er im ersten Fall zwecks einer schnellen Orientierung eine möglichst einfache Modellierung anwenden kann. Für die zweite Aufgabe jedoch dürfen aufwendigere Algorithmen in Betracht kommen, sofern sie auf realistischen Materialmodellen basieren und sofern hohe Ansprüche an Wirklichkeitsnähe gestellt sind.

2. STEIFIGKEITS- UND DÄMPFUNGSÄNDERUNG BEI STAHLBETONBAUTEN

Während mit Steifigkeit die Federungseigenschaften des schwingenden Systems angesprochen werden, repräsentiert der Begriff "Dämpfung" die Energiedissipationsfähigkeit des Tragwerks, nämlich die Umwandlung der Bewegungsenergie in nichtreversible Energieformen. Im folgenden wird sie durch das Verhältnis der nicht reversiblen Energie zur Gesamtverformungsenergie erfaßt. Um die Frage beantworten zu können, wie diese dynamischen Kenngrößen beim Werkstoff Stahlbeton im Gebrauchs- bzw. ganzen Tragfähigkeitsbereich eines Rahmentragwerks variieren, wurden in [3] Erdbebensimulationsversuche an Stahlbetonversuchskörpern durchgeführt. Dabei wurden repräsentative Tragwerksteile, wie Stahlbetonstützen und -rahmen in mehreren Laststufen, mit steigenden Amplituden für horizontale Bodenbewegungen, bis zum Versagen beansprucht (Fig. 1).

In der mit dem Beginn der Rißentwicklung einsetzenden nichtlinearen aber noch fast elastischen Anfangsphase verlieren die vorwiegend auf Biegung beanspruchten Bauteile mit fortschreitender Rißbildung deutlich an Biegesteifigkeit (Fig. 2). In den Kraft-Verformungszyklen wird ein Verfestigungscharakter bei größer werdenden Amplituden beobachtet. Ursache dafür sind die plastischen Relativverschiebungen des Stahls gegen den Beton (Schlupf) in rißnahen Bereichen. Beim nahezu linear-elastischen Verformungsverhalten des Stahls und des Betons steigt die ursprünglich aus reiner Materialdämpfung im elastischen Zustand bestehende Energiedissipation infolge plastischer Verbundeigenschaften und infolge Reibung entlang der Rißufer im Beton an.

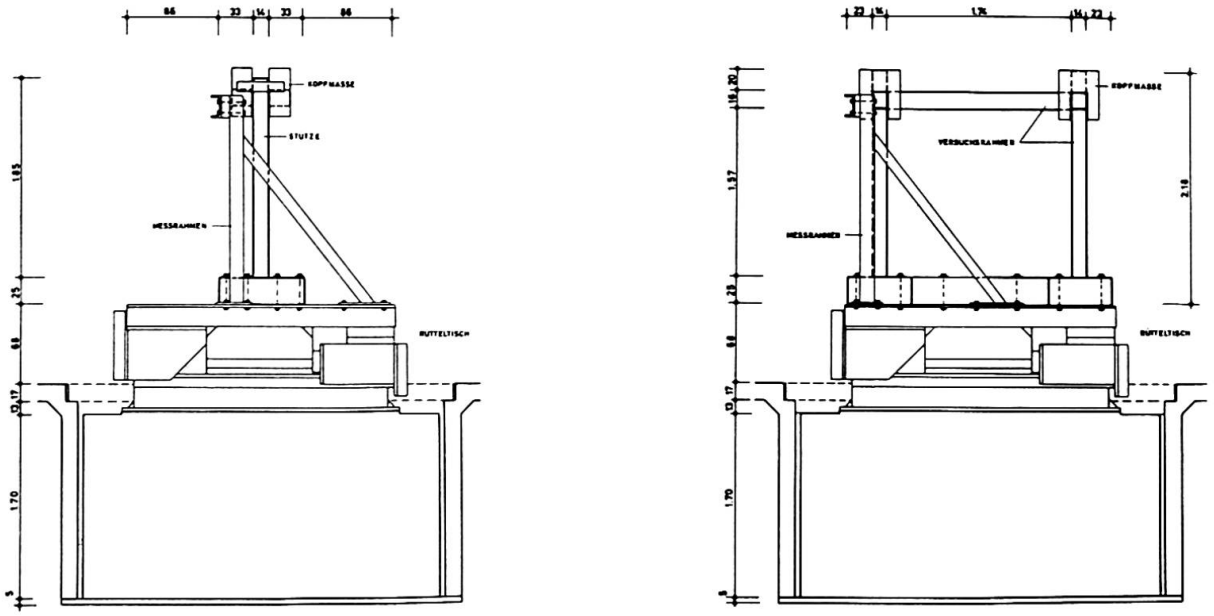

Fig.1 Erdbebensimulationsversuch mit Stahlbetonkragarm und -rahmen

Die plastische Formänderung des Bewehrungsstahls führt bei einer Beanspruchung über die Fließgrenze hinaus zu einem nichtlinearen, plastischen Bauteilverhalten. Die Zyklen weisen im Bereich großer Verformungen eine abnehmende Steifigkeit auf (Fig. 3). Die Energiedissipation wächst mit zunehmenden plastischen Verformungen und erreicht Werte, die ein Vielfaches der Werte in der elastischen Phase betragen. Abnehmende Steifigkeit im Stahl und Abplatzen der Betondeckung bei größeren Rotationen verschlechtern die Festigkeitseigenschaften in der Druckzone. Mit Abnahme des inneren Hebelarms sinkt auch das aufnehmbare Moment. Wird das noch vorhandene Arbeitsvermögen des Bauteils durch die zugeführte Energie überschritten, so versagt der Träger.

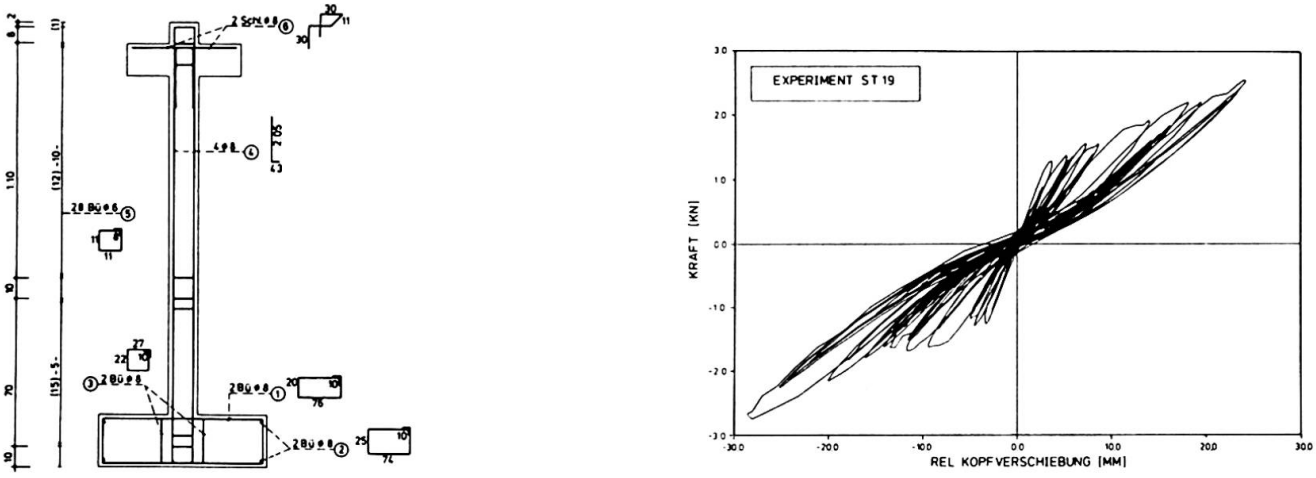

Fig.2 Nichtlinear-elastisches Bauteilverhalten des Stahlbetonkragarms

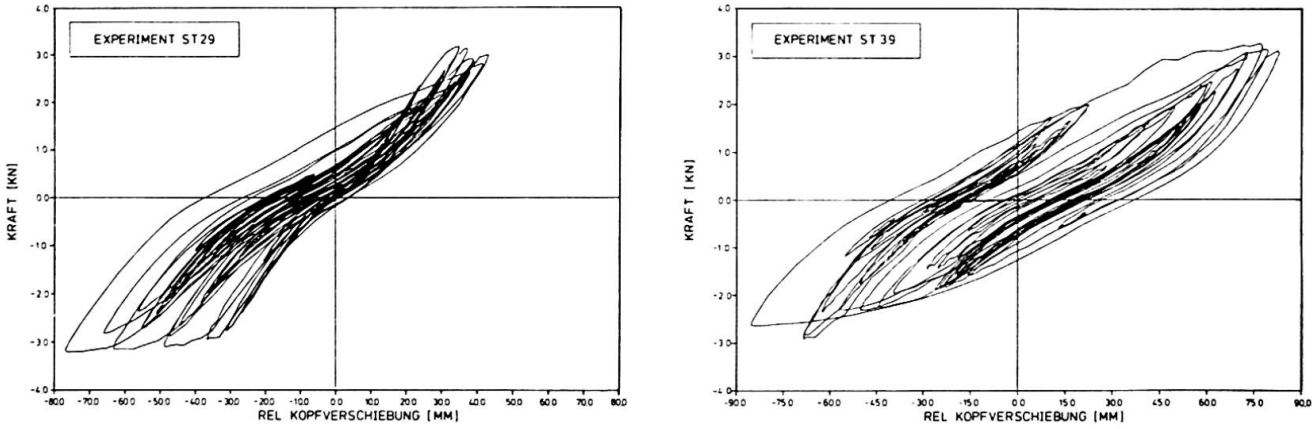

Fig. 3 Nichtlinear-plastisches Bauteilverhalten des Stahlbetonkragarms

3. MODELLIERUNG DER STEIFIGKEITS- UND DÄMPFUNGSÄNDERUNG

Mit welcher Genauigkeit und mit welchem Rechenaufwand das Werkstoffverhalten modelliert werden soll, hängt mit der jeweiligen Aufgabenstellung zusammen, wie bereits im ersten Abschnitt diskutiert wurde:

Stellt sich die Aufgabe als eine Dimensionierungs- und Bemessungsaufgabe, so wird man von einer tolerierbaren Schädigung ausgehend durch integrale Größen, wie z.B. Energie (Vergleich der aufnehmbaren und der aufzunehmenden), eine schnelle Orientierung suchen.

Ist dagegen eine genauere Kenntnis über die Tragwerksantwort erforderlich, z.B. zwecks Nachweis der Erfüllung bestimmter Sicherheitsanforderungen bzw. Lokalisierung von plastischen Verformungen auf bestimmte Tragwerksteile, so ist ein genaueres und dafür aufwendigeres Bauteilmodell notwendig. Nur sollte sich dies auf experimentellen Untersuchungen gründen und die Funktionsweise für den Anwender nachvollziehbar bleiben. Sein Anwendungsbereich soll möglichst deutlich angegeben werden. Innerhalb seiner Anwendungsgrenzen sollen fundamentale Werkstoffbeziehungen benutzt und damit die Eingabe dem Benutzer leicht gemacht werden.

Im folgenden wird zunächst ein solches werkstoffgerechtes Modell für das dynamische Verhalten schlanker, hauptsächlich biegebeanspruchter Rahmenbauteile vorgestellt. Das Modell basiert auf der systematischen Identifikation und Synthese der Einzelphänomene bei Versuchen, die im Kap. 2 zusammengefaßt wiedergegeben wurden. Dann wird ein vereinfachtes Rechenmodell präsentiert, welches dem Ingenieur als eine praxisfreundliche und zuverlässige Beurteilungshilfe für die werkstoffbedingten Tragwerkseigenschaften bei erdbebenbeanspruchten Stahlbetonrahmen dienen soll.

3.1 Werkstoffgerechte Modellierung

Wird das in Fig. 4 dargestellte idealisierte Tragwerksmodell einer horizontalen Bodenbeschleunigung ausgesetzt, so erhält man in den einzelnen Bauteilen einen vorwiegend linearen Momentenverlauf mit nur einem Nullpunkt. Es wird ersichtlich, daß jedes Bauteil aus zwei Kragarmen zusammengesetzt werden kann. Hat man ein Modell für den Kragarmmodul, das sein dynamisches Verformungsverhalten beschreibt, so kann mit den Mitteln der Stabstatik das ganze Tragwerksverhalten beschrieben werden.

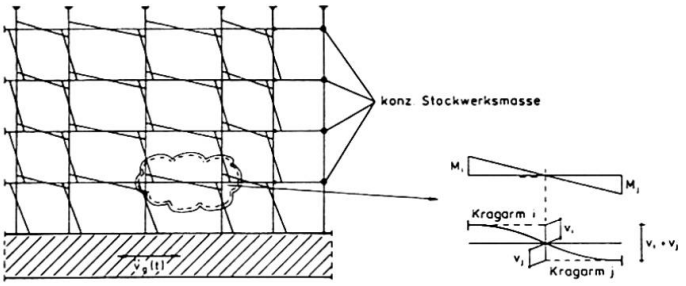

Fig.4
Idealisiertes Tragwerksmodell unter Erdbebenerregung

Beginnend mit dem ungerissenen Zustand wird in [3] der vollständige Tragfähigkeitsbereich des zähen Kragarms in drei Phasen zusammengefaßt:1.)linear-elastisch; 2.)nichtlinear-elastisch; 3.) nichtlinear-plastisch. Beim ersten Riß vollzieht sich der Übergang von der ersten Phase in die zweite und beim Fließbeginn im Bewehrungsstahl der Übergang in die dritte Phase (Tabelle 1).

- Die linear-elastische Phase ist durch eine konstante Steifigkeit charakterisiert, mit der das Bauteil unabhängig von der Lastspielzahl auf Be- und Entlastung reagiert. Die im Kraft-Verformungs-Diagramm umschlossene, recht schmale Fläche reflektiert die Energiedissipation infolge des vorwiegend thermo-elastischen Energietransfers. Bildet man sie äquivalent viskos ($c_{äq}$) ab, so kann mit einer einheitlichen Steifigkeit K_o für Be- und Entlastung gerechnet werden.

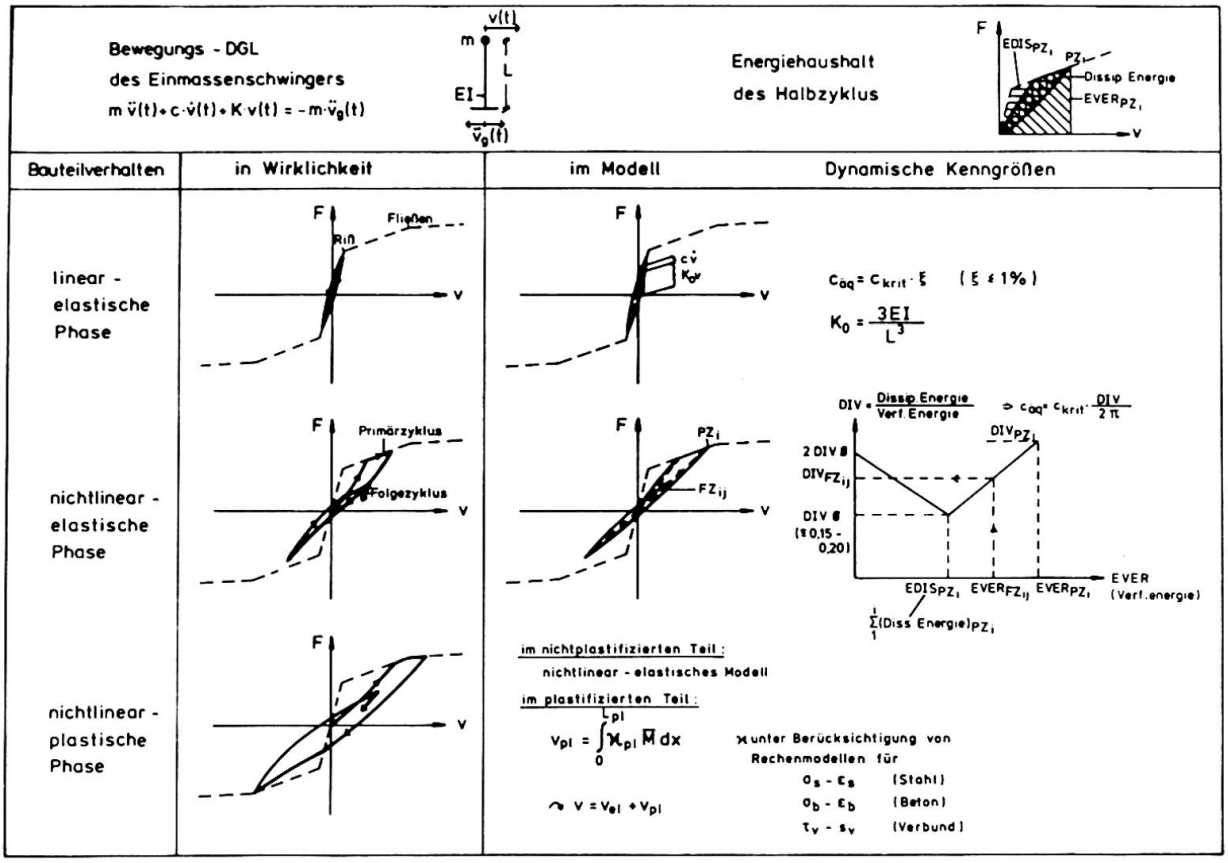

Tabelle 1 Prinzipien der werkstoffgerechten Modellierung

Die nichtlinear-elastsiche Phase ist durch einen Steifigkeitsabbau gekennzeichnet. Um diesen Schädigungsprozeß einfach beschreiben zu können, wird für die Zyklen folgende Klassifizierung vorgenommen: Im Beobachtungszeitraum i werden der Zyklus mit der bisher größten Verformungsamplitude Primärzyklus PZ_i und die ihm folgenden Zyklen mit kleineren Amplituden Folgezyklen FZ_{ij} genannt. Bildet man mit der veränderlichen Steifigkeit K die rissebedingte Schädigung des Bauteils bei Beanspruchungssteigerung durch die Primärzyklen und die dazwischen konstant bleibenden Stiefigkeitseigenschaften mit Hilfe der Folgezyklen ab, so wird eine recht gute Annäherung an das tatsächliche Kraft-Verformungsverhalten erreicht.

Die einfachen Be- und Entlastungsregeln für PZ erfassen dabei die mit der Rißentwicklung korrespondierende Energiedissipation. Aber auch dem Dissipationsvorgang in den Phasen ohne Rißentwicklung, d.h. zwischen den Primärzyklen, kommt eine Bedeutung zu, weil er die Phasenbeziehung zwischen der Erregung und der Antwort beeinflußt. In der Tabelle 1 wird ein Modell vorgestellt, das sowohl den Schädigungsgrad als auch die aktuelle Amplitude des betrachteten Folgezyklus berücksichtigt und die Energiedissipation äquivalent viskos ($c_{äq}$) abbildet. Dabei dienen die Primärzyklus-Energien $EVER_{PZi}$ (Verformungsenergie im zug. Primärzyklus) und $EDIS_{PZi}$ (Summe der dissipierten Energie in den bisherigen Primärzyklen) als Schadenskenngrößen zur Bestimmung von $c_{äq}$ eines jeden Folgezyklus FZ_{ij} .
In der nichtlinear-plastischen Phase entfalten die einzelnen Werkstoffkomponenten (Stahl, Beton, Verbund) bei zunehmenden Verformungen ihre Nichtlinearitäten und Plastizitäten so stark, daß ein globales Verhaltensschema für das Bauteil nicht realistisch formulierbar ist.

Hier hilft nur eine konsequente Berücksichtigung der $\sigma - \varepsilon$ - Beziehung für Stahl und Beton und der $\tau - s$ - Beziehung für Verbund, die unter Einhaltung von Gleichgewichts- und Verträglichkeitsbedingungen in einigen Schnitten diskret verfolgt werden. Die Superposition der einzelnen Beiträge liefert eine Information über den vom Plastifizieren erfaßten Bauteilabschnitt. Der mit dieser Vorgehensweise verbundene Rechenaufwand kann durch entsprechende Wahl der Anzahl der Schnitte gesteuert werden.

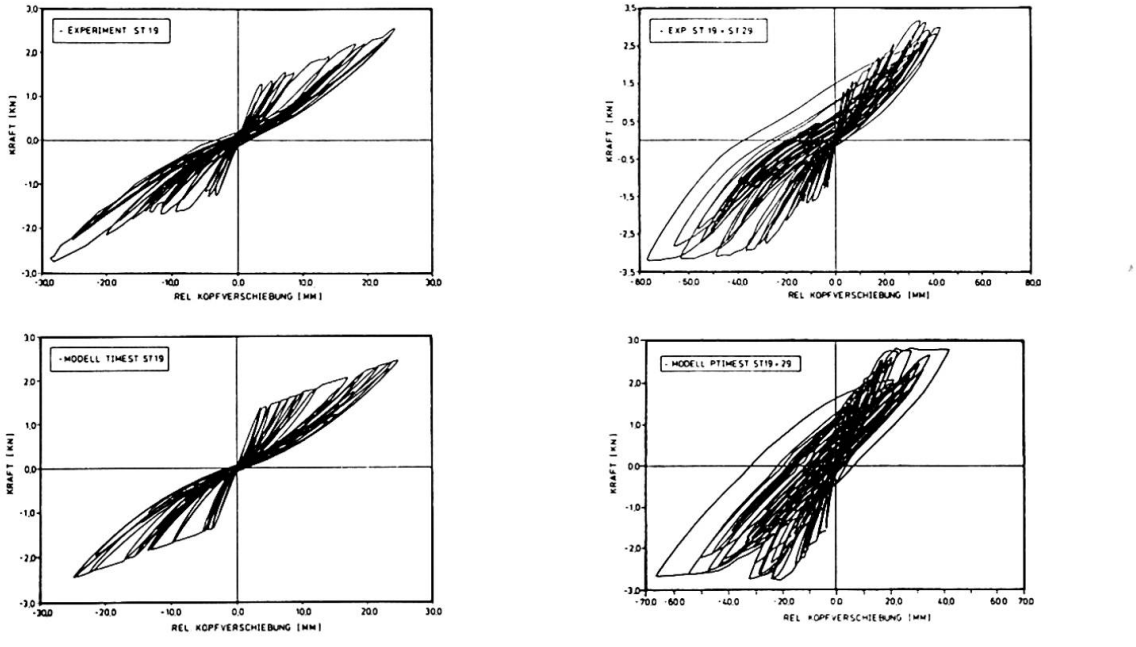

Fig.5 Vergleich zwischen Experiment und Berechnung mit werkstoffgerechtem Modell

Das oben präsentierte Modell wurde in [3] in eine Zeitschrittmethode mit direkter Integration der DGL implementiert. Bei der Nachrechnung der im Kap. 2 beschriebenen Erdbebenversuche an einfachen Stahlbetontragwerken zeigte das Modell eine gute Übereinstimmung. In Fig. 5 sind die Vergleiche von Experiment und Berechnung eines Kragarm-Versuchs in aufeinanderfolgenden Beanspruchungsstufen dargestellt.

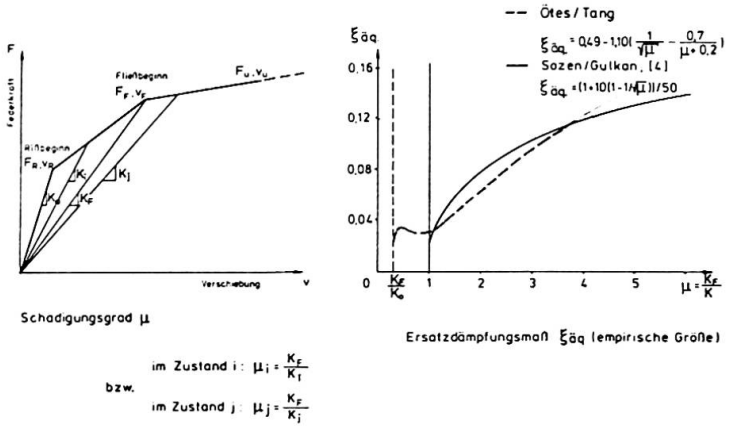

Fig.6 Linearisierte Kraft-Verformungsbeziehung und Ersatzdämpfungsmaß

3.2 Vereinfachte Modellierung

Ausgehend von der monotonen Kraft-Verformungsbeziehung des Bauteils mit linearisierten Be- und Entlastungsästen kann versucht werden, die Steifigkeitsreduktion durch den sog. Schädigungsgrad $\mu = K_F/K$ (K_F = Steifigkeit beim Fließbeginn) zu beschreiben (Fig. 6). Zusätzlich wird eine empirische Beziehung, die den Zusammenhang zwischen dem Schädigungsgrad μ und der korrespondierenden Energiedissipation $\xi_{äq}$ direkt wiedergibt, herangezogen (Fig. 6). Mit beiden Beziehungen wird die Möglichkeit geschaffen, das praxisfreundliche Antwortspektrum mit realistischen Eingangswerten zu benutzen. Diese bereits in [4] für die Bemessung zäher Rahmenkonstruktionen vorgestellten Näherungsmodelle werden im folgenden ergänzt (Fig. 7):

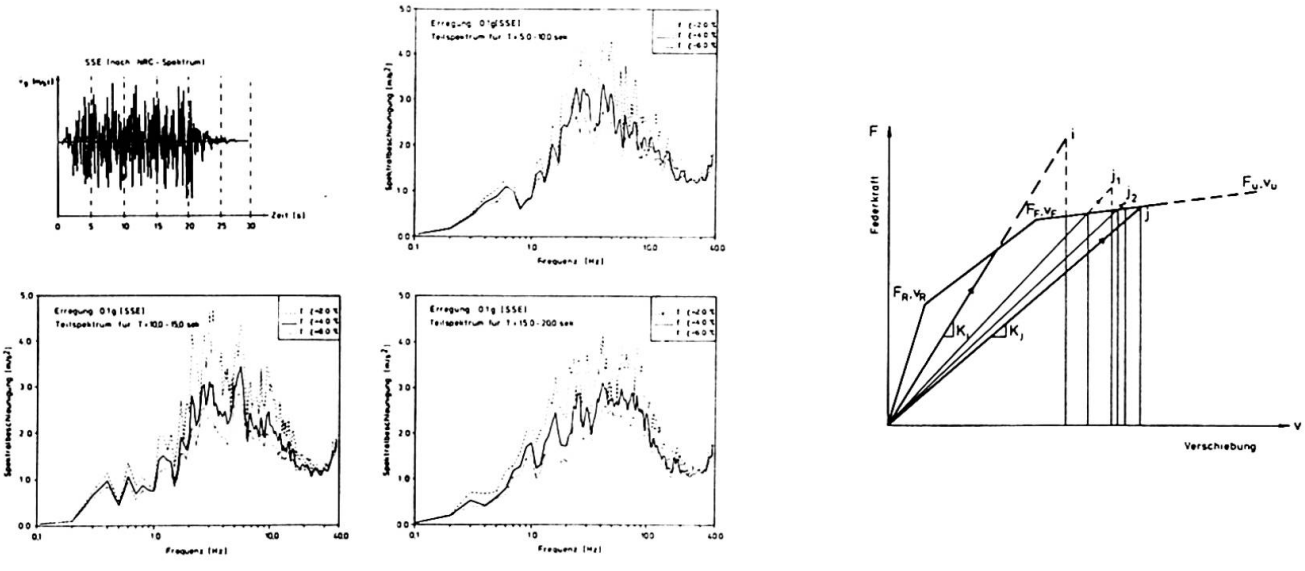

Fig.7 Teilantwortspektren und Energievergleichsmethode

- Benutzung von Teilantwortspektren statt des gesamten Antwortspektrums: So kann das zeitlich veränderliche Beanspruchungsbild, wenn auch in großen Intervallen, im Hinblick auf Auswirkungen auf Werkstoff- und damit Bauteilkenngrößen besser rekonstruiert werden. Mit Hilfe der Maximalantwort im betrachteten Teilantwortspektrum wird zunächst die Frage beantwortet, ob die Schädigung zunimmt. Im Falle einer Zunahme werden die Steifigkeits- und Dämpfungseigenschaften aktualisiert. Mit diesen aktualisierten dynamischen Kenngrößen wird die Berechnung im nächsten Teilspektrum fortgesetzt.
- Implementierung einer modifizierten Energievergleichsmethode zur Umrechnung der linear absorbierten Energie (E_i) in das nichtlinear-plastische System: Die für den Zustand i im betrachteten Teilantwortspektrum abgelesene Spektralbeschleunigung $S_{a,i}(f_i,\xi_i)$ führt zu der absorbierten Energie E_i. Sie ist für Beanspruchungen, die über das gegebene Kraft-Verformungsdiagramm hinausgehen, ein theoretischer Wert. Daher wird sie bei der Ermittlung der vom nichtlinear-plastischen System absorbierten Energie nur als eine erste Näherung benutzt. Aus $E_{j,1} = E_i$ folgen der Schädigungsgrad $\mu_{j,1}$ und das zug. Ersatzdämpfungsmaß $\xi_{j,1}$. Liegt die Antwort des linearen Schwingers j,1 im gleichen Teilantwortspektrum nicht auf der F-v Linie, so wird die zug. absorbierte Energie ($E_{j,1}$) wieder in eine F-v gerechte Energie ($E_{j,2}$) umgewandelt. Die Iteration kann abgebrochen werden, wenn ein Schädigungsgrad erreicht wird, bei dem die lineare Systemreaktion einen mit dem F-v Diagramm verträglichen Energiehaushalt aufweist.

In Fig. 8 ist ein Vergleich zwischen dem so entwickelten Teilspektrenverfahren und einem Kragarm-Versuch in einigen aufeinanderfolgenden Beanspruchungsstufen dargestellt.

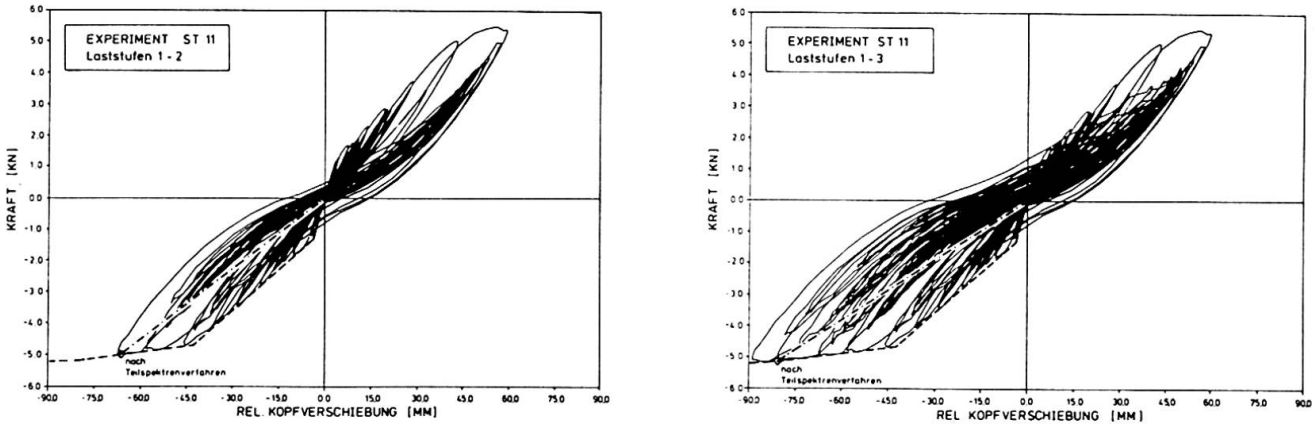

Fig.8 Vergleich zwischen Experiment und Näherungsverfahren

LITERATURVERZEICHNIS

1. CEB Model Code for Seismic Design of Concrete Structures, Comite du Beton, Bulletin D'Information No 160, 1983
2. TASSIOS T.P., et al., Response of R.C. Critical Regions Under Large Amplitude Reversed Actions, CEB-Bulletin D'Information No 161, 1983
3. KÖNIG G., KROGGEL O., ÖTES A., Untersuchungen zum nichtlinearen Verhalten erdbebenbeanspruchter Stahlbetonkonstruktionen, Abschlußbericht, Teil I: BMFT-RS-150444; Teil II: BMFT-RS-1500444 A9, Sept. 1983
4. SHIBATA A., SOZEN M.A., Substitute Structure Method for Seismic Design in R/C. Journal of the Structural Division, ASCE, Vol. 102, No. ST1, 1976